Applied Materials Today 20 (2020) 100772

Contents lists available at ScienceDirect

Applied Materials Today

journal homepage: www.elsevier.com/locate/apmt

Hierarchical fibrous structures for muscle-inspired soft-actuators: A review

Carlo Gotti[a], Alberto Sensini[b], Andrea Zucchelli[a,b,*], Raffaella Carloni[c], Maria Letizia Focarete[d,e]

[a] Department of Industrial Engineering, Alma Mater Studiorum—University of Bologna, I-40131 Bologna, Italy
[b] Advanced Mechanics and Materials – Interdepartmental Center for Industrial Research (CIRI-MAM), Alma Mater Studiorum—University of Bologna, I-40123 Bologna, Italy
[c] Faculty of Science and Engineering – Bernoulli Institute for Mathematics, Computer Science and Artificial Intelligence, University of Groningen, Nijenborgh 9 9747 AG, Groningen, The Netherlands
[d] Department of Chemistry 'Giacomo Ciamician' and National Consortium of Materials Science and Technology (INSTM, Bologna RU), Alma Mater Studiorum—University of Bologna, I-40126 Bologna, Italy
[e] Health Sciences and Technologies—Interdepartmental Center for Industrial Research (CIRI-HST), Alma Mater Studiorum—University of Bologna, I-40064 Ozzano dell'Emilia, Bologna, Italy

ARTICLE INFO

Article history:
Received 24 March 2020
Revised 12 June 2020
Accepted 19 July 2020

Keywords:
Soft robotics
Nanostructured materials
Artificial muscles
Bioinspired structure
Linear fibrous actuators

ABSTRACT

Inspired by Nature, one of the most ambitious challenge in soft robotics is to design actuators capable of reaching performances comparable to the skeletal muscles. Considering the perfectly balanced features of natural muscular tissue in terms of linear contraction, force-to-weight ratio, scalability and morphology, scientists have been working for many years on mimicking this structure. Focusing on the biomimicry, this review investigates the state-of-the-art of synthetic fibrous, muscle-inspired actuators that, aiming to enhance their mechanical performances, are hierarchically designed from the nanoscale up to the macroscale. In particular, this review focuses on those hierarchical fibrous actuators that enhance their biomimicry employing a linear contraction strategy, closely resembling the skeletal muscles actuation system. The literature analysis shows that bioinspired artificial muscles, developed up to now, only in part comply with skeletal ones. The manipulation and control of the matter at the nanoscale allows to realize ordered structures, such as nanofibers, used as elemental actuators characterized by high strains but moderate force levels. Moreover, it can be foreseen that scaling up the nanostructured materials into micro- and macroscale hierarchical structures, it is possible to realize linear actuators characterized by suitable levels of force and displacement.

1. Introduction

Bioinspiration is getting an increasing attention in the production of innovative robotic actuating systems [1,2]. In particular, the last decade has seen the outstanding arise of bioinspired structures in the field of soft robotics [3]. The main aim that distinguishes

Abbreviation: ATP, adenosine triphosphate; PVC, polyvinyl chloride; PVA, polyvinyl alcohol; DC, direct current; NFES, near field electrospinning; CVD, chemical vapour deposition; CNTs, carbon nanotubes; PANi, Polyaniline; PAN, Polyacrylonitrile; PPy, polypyrrole; PEDOT, Poly(3,4-ethylenedioxythiophene); PES, polyester; PVDF, polyvinylidene fluoride; MM, molecular motors; PAA, polyacrylic acid; PET, polyethylene; PU, polyurethane; GO, graphene oxide; Nb, niobium; PEVA, poly(ethylene-co-vinyl-acetate); MWCNT, multi walled carbon nanotube; Pt, platinum; Ag, silver; Au, gold; C, carbon; Sn, tin; Al, aluminium; Cu, copper; p-TSA, para-toluene sulfonic acid; NaDBS, dodecylbenzene sulfonate; PDDA, Poly (diallyl dimethylammonium chloride); TPU, thermoplastic polyurethane; PVDF-co-HFP+TEA·BF4, Poly (vinylidene fluoride-co-hexafluoropropylene) + tetraethyl ammonium tetrafluoroborate; PVA+H2SO4, polyvinyl alcohol + sulfuric acid; TBA·PF6, tetrabutylammonium hexafluorophosphate; AFM, atomic force microscope; TEM, transmission electron microscopy; UV, ultra-violet light; CCD, charge-coupled device; $CaCl_2$, calcium chloride; 2-ply, two-ply; 4-ply, four-ply; SMP, shape memory alloy; Inox, stainless steel; SMC, shape memory ceramics; TCP, twisted and coiled polymers; UHMWPE, ultra-high molecular weight polyethylene.

* Corresponding author at: Department of Industrial Engineering, School of Engineering and Architecture, University of Bologna, Viale Risorgimento, 2 40136 Bologna, Italy
E-mail addresses: carlo.gotti@unibo.it (C. Gotti), alberto.sensini2@unibo.it (A. Sensini), a.zucchelli@unibo.it (A. Zucchelli), r.carloni@rug.nl (R. Carloni), marialetizia.focarete@unibo.it (M.L. Focarete).

https://doi.org/10.1016/j.apmt.2020.100772

this branch of robotics is to design a new generation of compliant actuators able to mimic the skeletal muscle performances.

Skeletal muscles properties mainly rely on their hierarchical structure, composed of fibrous actuators organized in different levels of aggregation. This structure can produce force by the shortening of their elementary contractile units, the sarcomeres, making muscles classifiable as linear actuators. This complex organization also permits a fine control on the separate activation of their subunits, conferring them a high scalability and modularity. This linear shortening, matched with the skeletal lever system, allows a wide range of motions with a controllable stiffness, also reducing the muscle clutter. Considering all these properties and the perfectly balanced mechanical performances, the skeletal muscle is considered the best actuator in Nature [4].

Aiming to mimic skeletal muscles and the features listed above, several innovative strategies were investigated to obtain synthetic soft-actuators, such as smart textiles, additive manufactured devices, shape memory alloys, pneumatic, hydrogel composites, origami / kirigami structures and many others, revolutionizing the field of the classic robotics [3,5–8]. Among these, some works tried to faithfully reproduce the hierarchical morphology of muscles and their linear actuation, by using scalable and modular fibrous structures [173]. This approach will be of extreme interest for all those applications in which a biomimetic load transfer matched with reduced weight, clutter and high softness are required, such as in advanced surgical instrumentations, orthosis, prosthetic devices, exoskeletons and biologically-inspired robots [9–17]. In this review we purposely focus only on linear actuators with fibrous structure and nano or micro dimensions, considered eligible to be arranged in a bioinspired hierarchical fashion, enhancing their force and strain capabilities with the same strategies chosen by the evolution in the biological skeletal muscles.

The paper is organized as follows. A brief review of the morphology, mechanical properties and physiology of skeletal muscles is given in chapter 1. In chapter 2, the most common features that are required for a muscle-inspired soft-actuator are investigated. The main technologies for nano- and microfibers production are presented in chapter 3 along with, in chapter 4, the most frequently employed materials for artificial muscles production. In chapter 5, an analysis of the state-of-the-art of muscle-inspired actuators is presented. Specifically, chapter 5 is divided in four sections, depending on the hierarchical level of complexity of the actuator: single fibers, flat mats of fibers, bundles/yarns and finally coiled and/or plied structures. For each work cited in this chapter, the structure proposed by authors, the material used, the manufacturing process and the principal outcomes are summarized. Finally, concluding remarks are drawn in chapter 6.

1.1. Hierarchical morphology of skeletal muscles

A skeletal muscle is an organ mainly composed of striated muscular tissue. It is the major actuator of human body, providing its movement capabilities, being composed of contractible cells called myocytes. A skeletal muscle has three other main functions: to support the body, to generate heat during contraction, and to protect bones and organs. It is the only type of muscle tissue classified as voluntary, whose contraction is regulated by our conscious cerebral activity. It is also called striated muscle because it alternates light and dark bands, which are visible under the optical microscope. Skeletal muscles form about 40% of the entire body weight and they are made up of water (75%), proteins (20%) and other substances, such as salts, minerals, fat, and carbohydrates (5%) [18]. The protein content mainly consists of collagen (Type I, III, IV and V) for the tissue sheaths [19], and myosin, actin, titin and nebulin for the inner parts [18]. It is a composite structure, made by contractile materials and, in minor amount, by blood vessels, nerves and connective tissue [20,21]. The skeletal muscle shows a hierarchical architecture of aligned structures like other connective tissues, such as tendons and ligaments.

The fundamental building-block of the skeletal muscle is the sarcomere, which is composed of different filamentous proteins, called myofilaments (Fig. 1A) [22]. Sarcomeres are connected through a plate-shaped region of dense protein material, called the Z-line. The myofilaments are divided in thick, thin, and elastic ones. Thin and thick filaments overlap on each other with a process called sliding mechanism [22]. This is the mechanism that the muscle employs to shorten itself and produce a contractile force. The amount of overlapping depends on the muscle level of contraction. Thick filaments are made of about 200 myosin molecules and have a diameter of about 16 nm [18]. Thin filaments are placed on the side of the thick ones and extend from the Z-lines to the beginning of the H-zone, the region in which no overlaps with thick filaments are present. Thin filaments are made of actin molecules joined together in a helix pattern, with a small amount of two proteins called tropomyosin and troponin. The elastic filament is composed of the titin protein and links the thick filaments to the Z-line. The titin function is to stabilize and confer an elastic recovery to the myosin [23]. This overlapping of myofilaments provides the typical striated appearance to skeletal muscles (Fig. 1B). Sarcomeres are connected each other both in a parallel and longitudinal way. Thousands to millions of these sarcomeres form an upper level structure called myofibril (Fig. 1B). Myofibrils have a mean diameter of 1-2 μm. Several myofibrils, parallelly arranged and wrapped inside a sheath of connective tissue called endomysium, produce the muscle fiber (Fig. 1C). Endomysium is primally composed by collagenous fibers (Type I, III, IV, V) [19]. Each muscle fiber has a mean diameter of 10-100 μm with a typical length of 1 cm [18] and can be considered the biological structural unit of skeletal muscles, consisting in a single, multinucleated cell called myocyte. Moreover, the whole size of the muscle is determined by the number and dimension of its individual muscle fibers [18]. The cell membrane of these fibers is named sarcolemma and surrounds its cytoplasm or sarcoplasm. Excluding their water content, muscle fibers are mainly (80%) composed of proteins (classified by specific function such as contractile, regulatory, and cytoskeletal ones) and sarcoplasm (8%) [18]. Being a cell, the muscle fiber is irrorated by capillaries and connected with nerves through neuromuscular junctions. Inside and around the muscle fiber a membrane-bound structure, the sarcoplasmic reticulum, is found [24]. Its main function is to store calcium ions (Ca^{2+}) which are essential for contraction. Sarcoplasmic reticulum presents also enlarged areas named terminal cisternae, that surround introflexions of the cellular membranes (i.e. T-tubules) inside the fiber. Bundles of muscle fibers form a muscle fascicle (Fig. 1D). This structure is surrounded by another connective tissue sheath, the perimysium, composed of Type I, III and V collagen fibers [19]. Groups of fascicles, bundled together, generate the whole muscle belly (Fig. 1E). The whole muscle is coated by a layer of dense, irregular connective tissue sheath named epimysium. This membrane is primally made of large collagen filaments (Type I and III). The terminal side of the muscle progressively changes composition, increasing the collagen amount and decreasing the cellular part, becoming a tendon that connects the muscle to a bone [25].

1.2. Skeletal muscles mechanical properties and contraction mechanism

The mechanical properties of skeletal muscles can be divided in two categories: the passive ones, which depend only on the tissue mechanical response while stretched; and the active ones, which are derived from the activation of the contractile elements. The in-

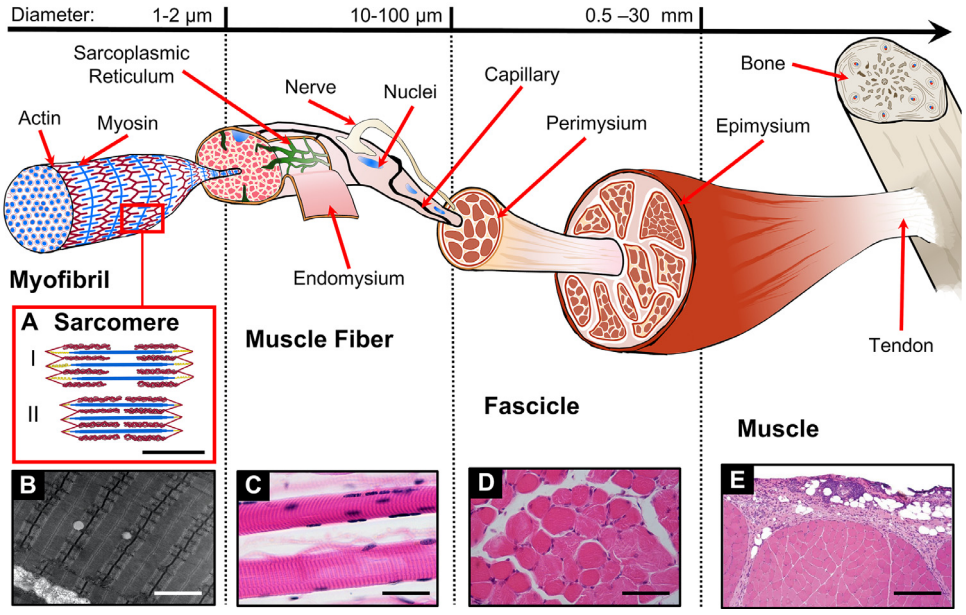

Fig. 1. Hierarchical structure of skeletal muscle. A) Sarcomere morphology and sliding mechanism (Scalebar 0.5 nm): Actin (red), Myosin (blue) and Titin (yellow) filaments are shown in the relaxed state (I) and during the contraction (II). The jagged sides represent the Z-lines. The central space without actin filaments is the H zone. B) Transmission Electron Microscopy (TEM) image of myofibrils (scalebar = 1 nm. Reproduced under CC0 1.0 Universal Public Domain Dedication. Author: Louisa Howard). C) Phase Contrast Microscope (PCM) image of skeletal muscle fibers. Dark violet elliptical elements are the myocytes nuclei (scalebar = 50 μm. Reproduced under CC0 1.0 Universal Public Domain Dedication. Author: Berkshire Community College). D) Histological image of a fascicle cross-section. Larger white bands are the perimysium membranes. Circular structures are the muscle fibers, while the darker violet dots are the myocytes nuclei (scalebar = 100 μm. Reproduced under Attribution-ShareAlike 3.0 Unported. Author: Ganimedes). E) Histological image of a portion of muscle cross-section. In the upper part, the epimysium membrane is visible (scalebar = 0.5 mm. adapted from [170], reproduced under permission. Copyright 2008, Elsevier B.V.).

ternal biological structures that provide those properties are not always anatomically distinct [26].

Passive properties are often obtained imposing an artificial stretch to the muscle, avoiding the activation of the contractile elements. Due to the high variability of muscle tissue, caused by the differences between the species tested and the intra-species variability, the mechanical properties reported in literature vary widely. Furthermore, there are not conventional techniques to test the passive mechanical properties of these tissues, and this causes additional variability [27]. The passive properties of the muscle belly depend on the intramuscular connective tissues (epimysium, perimysium, endomysium) [22]. However, recent evidences suggest that muscle cells are also responsible for their passive mechanical properties [26,28]. Moreover, the titin, the most abundant component of elastic filaments, is nowadays considered the structure that mainly bears the passive stress inside a muscle [20,23,27,29]. The two main passive mechanical features of a skeletal muscle are:

i) Extensibility: the muscles ability to be macroscopically stretched until a certain limit without being damaged [22].
ii) Elasticity: the muscles ability to recover the initial shape and length after being stretched [22].

The most practical way to compare values from different types of muscles is to normalize their produced force to their cross-sectional area. This index is known as specific stress [30]. When an isolated muscle is stretched *in vitro* at different strains, the stress response can be plotted in a passive stress–strain curve, that exhibits the typical non-linear behaviour of soft connective tissues (Fig. 2A) caused by the progressive alignment of the fibers [31,32]. After a toe-region, the muscle starts to develop stress linearly (i.e. linear region) (Table 1) [23,26,27]. The slope of this curve region determines the module of elasticity of the muscle. The relaxed muscle shows also a time dependent viscoelastic behaviour [31,33]. Viscoelasticity is due to the mechanical properties of intracellular and extracellular proteins, like collagen. When stretched and held at constant length, the stress decreases over time to a plateau (stress relaxation) [26]. Otherwise, if stretched at constant stress over time, the muscle lengthens to a new value (creep). Muscles also show different stress-strain curves if stretched and relaxed repeatedly [26].

The active mechanical properties of the skeletal muscle depend on its contractile behaviour. The two principal active properties of skeletal muscles are:

i) Excitability: the muscles ability to respond to a chemical stimulus, delivered by the release of a neurotransmitter by a nerve or a hormone, generating an action potential [22].
ii) Contractility: the muscles ability to generate a force and to produce a work by shortening. Muscles contract in response to one or more action potentials [22].

Being an actuator, the most important attribute of a muscle is the force that it can generate. The major determinant of the maximum potential force is the muscle size [47]. Human skeletal muscles show maximum active stress values in the range of 60-200 kPa [30,47]. These stresses are normally achieved during an isometric contraction, that occurs when the muscle generate force without changing its length. An important information about the muscle contraction is the relationship between the active stress and the sarcomere length (Fig. 2B) [22]. The skeletal muscle exerts stress when myosin (from thick filaments) connects to actin (from thin filaments) through cross-bridges. The muscle develops its maximum force when there is an optimal overlap between thin and thick filaments. When sarcomere length is about 2.2 μm (optimal length in humans, Lo) the force it can provide is maximum [22,27]. Further stretching the muscle results in a decrease of the contraction force and, when the sarcomere reaches about 175% of its optimal length, no force can be developed. The exerted stress is expressed as percentage of maximum active stress, achievable during a tetanic contraction. Muscle stress increases along with the stimulus frequency, until reaching a plateau that corresponds

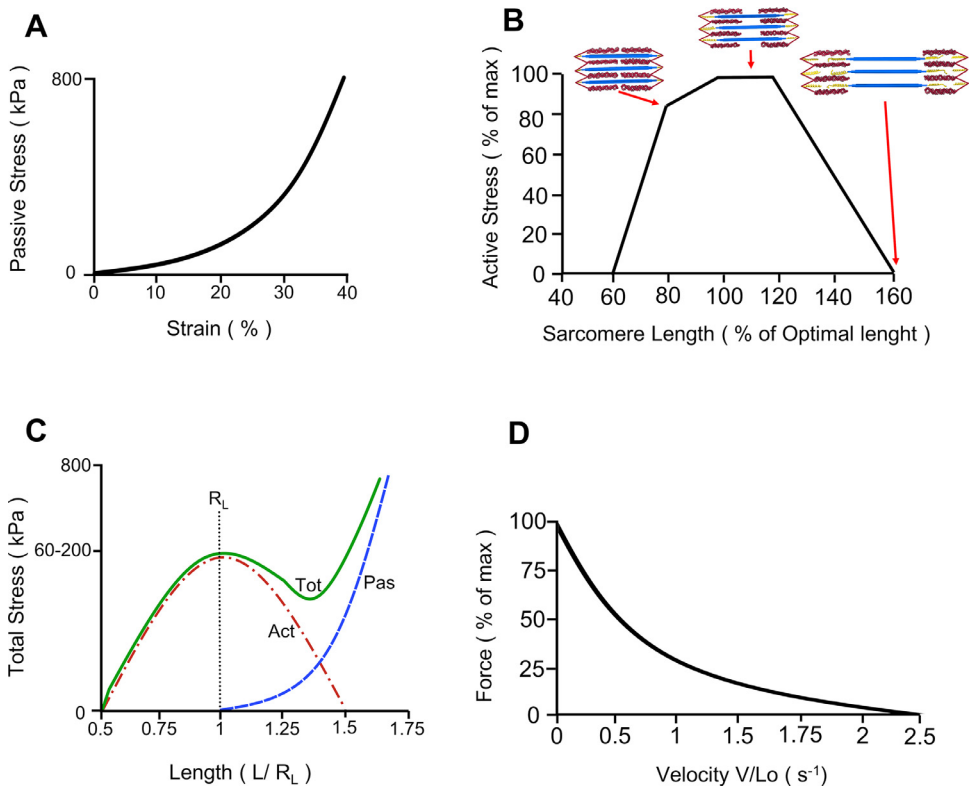

Fig. 2. Passive and active mechanical behaviours of skeletal muscles. A) Typical passive stress-strain curve. B) Typical sarcomere active stress (expressed as a percentage of the maximum) compared to the sarcomere length (expressed as a percentage of its optimal length). The active stress is maximum in correspondence of the sarcomere optimal length Lo. The pictures show the different levels of sarcomere overlap. C) Total stress-length behaviour during a contraction. Length is normalized by the resting length (R_L) of the muscle. The total curve (Tot) is the composition of the active curve (Act) and the passive one (Pas). The active curve finds its maximum in correspondence of the optimal length of the sarcomere (R_L). D) Typical force (expressed as a percentage of the maximum) compared to the speed of contraction (normalized by the optimal length of the sarcomere).

Table 1
Typical ranges of animal skeletal muscle passive mechanical properties.

	Elastic Modulus [kPa]	Failure Strain [%]	Failure Stress [kPa]
Myofibril	25-40 [34,35]	30-60 [36–38]	-
Fiber	20-100 [23,39–41]	30-60 [36–38]	430-1973 [42]
Whole Muscle	30-8000 [20,37,42–45]	30-60 [36–38]	70-800 [38,42,46]

to the maximum tetanic force [27]. The combination between the passive and the active mechanical properties generates the total stress-length relationship (Fig. 2C) [48].

Skeletal muscles are also able to regulate the force to be adequate to the load that they bear during the shortening. Moreover, a force-velocity relationship can describe the limits to muscle speed and force output [32]: for fast movements, the force produced by the contractile system is low, and vice versa (Fig. 2D) [49,50].

Skeletal muscles produce work only by contraction, reducing or holding the joint angle between the two bones to which they are connected through connective tissues (usually tendons). Being only able to contract, skeletal muscles usually work in pairs at the opposite side of a joint (in an antagonist setting) [2]. Each motor signal, originating into the motor neurons in the central nervous system, stimulates up to 1000 muscle fibers. The combination between a motor neuron and its connected fibers is called motor unit [24]. When the action potential has reached the axon terminal of the motor neuron, it promotes the release of chemical neurotransmitters at the neuromuscular junction. This complex is called synapsis [51]. When the neurotransmitter reaches the receptors located on the muscle side, they bind together causing the opening of sodium ions channels (Na^+). The related change in the fibers resting membrane potential triggers an electrochemical depolarization (i.e. action potential) that travels through the sarcolemma. The action potential passes into the muscle cell through T-tubules of the sarcoplasmic reticulum that stores calcium ions (Ca^{2+}). Then, voltage-gated channels located in T-tubules open, allowing an inward current of Ca^{2+}. This current further opens other channels, releasing a large amount of Ca^{2+} from sarcoplasmic reticulum cisternae. The Ca^{2+} high concentration removes the protein tropomyosin that inhibits the linking between the thin and the thick filaments. This process starts the filaments to slide one on each other, shorting the sarcomere [22]. The muscle contraction also requires energy for the sliding, obtained with the hydrolysis of the organic complex adenosine triphosphate (ATP), that binds to the myosin heads. The sarcomere shortening draws the Z-discs closer to each other, leaving the length of the filaments unchanged. When the contraction reaches the peak value, the sarcomere can decrease its length to a half. The relaxation occurs when the motor neuron stops to stimulate the fibers. The neurotransmitter is broken down and the muscular action potential is not generated anymore on the sarcolemma. Cell membrane ion transporters, called Ca^{2+} pumps, rapidly remove calcium and restore the original concentration, leaving tropomyosin able to bind again and inhibit the sliding.

The fibers contraction is an all-or-none activation [22]. When the fibers are reached by the action potential, they contract to their fullest extent. Muscles can perform graded contractions, with variable force, regulating the number of contracted fibers and their frequency of stimulation by the motor neurons. Relaxed skeletal muscles always present a few fibers in the contracted state to maintain the muscle firmness, which is named tone. If a skeletal muscle is overstimulated, it will rapidly lose strength. For this reason, during a contraction, not all fibers work. The pattern of firing of motor neurons changes, maintaining the contraction for longer periods by alternating the fibers involved. This prevents muscular fatigue at best, and it is also used to produce smooth movements instead of jerks [48].

Considering this, it is clear how the evolution aimed to enhance aspects like force, contraction ratio, activation control and fatigue resistance by exploiting the superposition concept in its hierarchical fibrous structures. Working in parallel, myofibrils, fibers and fascicles scale up the force output of the muscle, while sarcomeres, serially arranged, enhance the shortening during contraction.

2. Requirements for a muscle-inspired soft-actuator

The contractile mechanism and the hierarchical structure of skeletal muscles are drawing an increasing attention in the robotic research field, especially in the production of actuators.

A robotic actuator is defined as a device capable to transform energy, coming from any physical domain, to a motion by applying mechanical forces on a robotic joint, an object, or on the surrounding environment [52]. Nowadays, the actuation systems mainly rely on combustion, electric motors, or pneumatic/hydraulic. These technologies are well established and had been refined since their early discoveries around the middle of XIX century. However, to date, an established technology with properties similar to the skeletal muscle is still missing. This paragraph will focus on the process that brought researchers to investigate a new generation of artificial soft-actuators, trying to mimic the biological structure and the linear actuation system of skeletal muscles.

Actually, muscles do not overcome artificial actuators in any aspect [53]. For instance, both combustion and electric motors have higher specific power [54]. It is for their incredibly well balanced performance and features, and not for any single dominating characteristic, that muscles are considered the best existing actuator [4]. Force, for example, can be finely tuned with the recruitment mechanism, optimizing energy consumption, and refining movements. Muscles have also the ability to change their stiffness [53]. They convert chemical energy to mechanical one “combusting” ATP molecules, obtaining a fuel energy density up to two order of magnitude higher than artificial batteries [53]. Moreover, thanks to the hierarchical structure, skeletal muscles amplify the microscopic movements of the actin-myosin complex, obtaining macroscopic displacements [55].

Today, most of artificial actuator technologies are hard, non-compliant, heavy and noisy [52]. They have the advantage of being usually precise, fast and powerful when used in their specific application domain, but lack of adaptability when the environment of operation is not well known [56]. They, therefore, require complex transmission systems to be usable in non-repetitive tasks.

Nevertheless, in the last years, Nature has become more and more a source of inspiration for robotics and machines in general. Softness, compliance, and reduced complexity are key features often exploited in living beings. These features are also chased by robotic research to produce actuators capable to be used into unknown environments, overcoming the current drawbacks of classical ones [2,3]. This research culminated in the birth of a new class of systems, currently growing, referred as soft robots [57]. For the purpose of soft robotics application, a variety of emerging actuator technologies had been exploited [58,59]. Soft-actuators and, more specifically, artificial muscles, share some common generic requirements. Adequate stress and strain values should be exhibited to be of practical use. The strain rate (i.e. the average change in strain per unit time during an actuator stroke) should be sufficient to ensure a rapid responsiveness [53]. Other key-figures of merit are considered to evaluate artificial muscles, like the work density (i.e. the amount of work generated in an actuator cycle normalized by its volume), the specific power (i.e. the power output per unit mass) and the efficiency [53]. High reversibility and controllability would be also suitable [60], along with durability.

To satisfy these requirements with desired performances, many efforts have been made researching the employed materials. However, learning from Nature, it is clear how the geometrical and morphological structure of these materials is also fundamental when designing an artificial muscle. Working in the nanoscale it is possible to assemble nano-actuators and to scale up forces and contraction, mimicking the same approach of biological muscles [61]. Moreover, since most of researched actuators activation mechanisms rely on the inward electrolyte or heat perfusion, their power output tends to increase at smaller dimension due to faster mass, electronic and heat transport, or higher surface area to volume ratio. This is the choice “made” by the evolution for biological muscles and for this reason, solutions involving small-diameter actuating fibers had been proposed [62,63]. This approach is often limited by the laborious fabrication and sometimes by lacks in technology.

Another advantage brought by the mimicking of muscles could be the fine tuning of actuation force and stroke, in a similar way of the recruitment phenomenon. This mechanism is currently being investigated, through the exploiting of many textile architectures obtained using knitting, weaving, and braiding techniques [62]. For obvious morphological similarities, aligned fibers-structured artificial muscles would be favourable. High surface-to-volume ratios, along with high degree of porosity brought by the nano- or micrometric size gaps of fibrous hierarchical structures, could enhance their actuation performance and response [60,63,64].

To date, an unsolved topic in the soft robotics field is to realize flexible actuators capable to develop high forces, performances, and functionality by mimicking the hierarchical morphology of skeletal muscles in the animal body. These kinds of actuators are specially needed for assistive and rehabilitation devices that must safely physically interact with human beings [65], for example artificial limbs, prosthetic devices, exoskeletons, or even surgical instruments [3,66].

3. Technologies for nano- and microfibers production

In order to achieve fibrous hierarchically structured actuators, few manufacturing processes were chosen by researchers, which will be overviewed in this Section.

3.1. Spinning

Spinning is a manufacturing process involved in the production of polymer fibers. The three major techniques (melt spinning, dry spinning and wet spinning) are used for the production of most of commercial synthetic fibers, usually with a diameter in the micrometric or millimetric scale [67]. In order to produce fibers with diameters in the nanoscale, electrospinning or near-field electrospinning are usually employed.

3.1.1. Melt spinning (Extrusion)

The melt spinning is a widely used and well-established process in the manufactory industry (Fig. 3A). A bulk material is pushed through a die, creating objects with fixed cross-sectional profile.

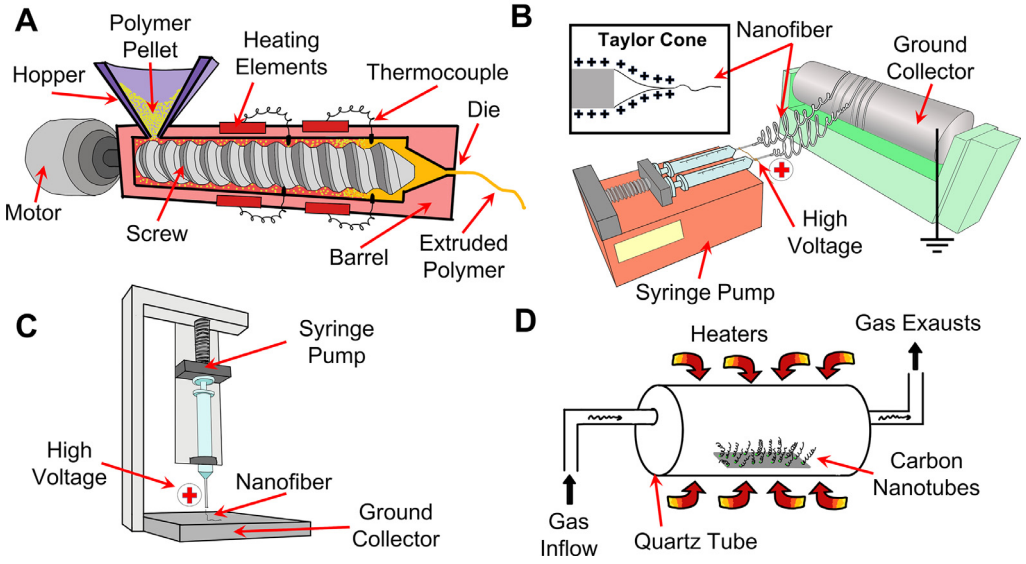

Fig. 3. Typical manufacturing processes employed in the production of microfibers and nanofibers: A) polymer melt spinning; B) electrospinning (the inset shows the Taylor cone); C) near field electrospinning; D) chemical vapour deposition.

The end-plate die determines the shape of the extruded material. When polymers are extruded, the raw material is stored into a hopper in the form of pellet and conveyed through a feeding screw to the die. During this process, the material is also heated with a controlled temperature. Extra-heat results also from the intense pressure and friction taking place between the screw, the material and the barrel. The continuous polymeric filament produced is then cooled by air or liquid [68]. Melt spinning process outcome depends on several parameters such as the polymer viscosity with its variations (due to shear stress and temperature), and its elasticity. Process parameters that should be monitored, are [68]:

i) Barrel temperature: it is usually chosen equal to the glass transition or the melting temperature of the polymer.
ii) Feed rate: it should be constant and linked to the screw speed. These two parameters are critical to obtain a homogeneous infill of the extrusion.
iii) Motor load and melt pressure: these parameters also depend on the feed rate and the screw speed, along with the molecular weight of the polymer.

Like in the microfabrication, the micro-scale melt spinning follows the same process [69]. Fishing line, for example, is usually made with an extruded polymer that had been melted, before being forced through a micro-scale hole.

3.1.2. Dry spinning

This methodology is employed for those polymers that need to be dissolved in a solvent, due to their thermal degradation temperature lower than the melting one. In the dry spinning, a volatile solvent is first used to dissolve the polymer into a solution. This solution is then purified by a filter and pushed through a spinneret into a warm air chamber to force the solvent evaporation. The polymer then solidifies into a thin filament that is wound around drums. The key variables of the dry spinning are the heat transfer, the mass transfer and the filament stress [67]. Common dry spun fibers include acrylics, polyvinyl chloride (PVC) and polyvinyl alcohol (PVA).

3.1.3. Wet spinning

This methodology is used, like dry spinning, for polymers that need to be dissolved to be spun. The solution is extruded through a spinneret directly into a chemical liquid bath. This causes the fiber precipitation and solidification. The solvent is then removed, and the filament is wound around a drum. The rate of extrusion is crucial to avoid micro-void formation into the fiber. Common wet spun fibers include acrylics, rayon, spandex, lyocell [70].

3.1.4. Electrospinning

The electrospinning process was developed in the early twentieth century [71] but, only in the last three decades, it has drawn increasing attention due to the exponential development of nanotechnologies [72]. This technique has proved to produce size-tuneable fibers in the nano- or micrometric scale and is widely employed to mimic the morphology of many biological tissues, such as tendons, ligaments, and muscles in the tissue engineering field [72–78].

The process is based on the stretching of a polymeric solution through a high electrostatic field (Fig. 3B). The system consists of a syringe with a thin metallic needle, loaded with the polymeric solution, a syringe pump to control the flow rate, and a metallic collector positioned at a certain distance. The needle is linked to the positive terminal of a direct current (DC) power supply, while the collector is grounded. The voltage applied is of several kilovolts (5–30 kV) [79]. This produce a high electrostatic field between the needle and the collector. Then, the solution droplet flowing out of the needle is stretched by the electrostatic field to form a conical shape, called Taylor cone (Fig. 3B). A jet stream emanates from the cone apex, firstly with straight trajectory, then with a whipping movement towards the collector. This motion induces the polymeric chains to stretch and the stream to shrink. This elongation, along with the evaporation of the solvent, produce a continuous fiber with a tuneable diameter from the nano to the macro scale [80–82]. The outcome of the electrospinning process depends on three families of parameters [72,80]:

- Solution parameters: the polymer(s) and the solvent(s) chosen, their concentration, conductivity, and viscosity [83].
- Process parameters: the applied electrostatic field, the needle–collector distance, the collector shape, the collector rotational speed, the flow rate and the needle diameter [84].
- Environmental parameters: the relative humidity and the temperature.

Tuning these parameters, different fiber morphologies, cross-sectional areas and porosities are attainable. By changing the shape

of the collector, it is also possible to introduce a preferential alignment of the fibers [71], reproducing the parallel arrangement of the skeletal muscle ones. This allowed to produce scaffolds (even resorbable) for muscle regeneration, able to guide the growth of different tissue cells [85–88]. For all these reasons, electrospinning is one of the most promising techniques also employed in the development of bioinspired muscle-like actuators.

3.1.5. Near field electrospinning

The near field electrospinning (NFES) is a spinning process where solid nanofibers are deposited in a direct, continuous and controllable way (Fig. 3C) [89]. "Near field" means that the process aims to deposit the nanofiber on the collector when it is still in the stable liquid jet zone. Conversely to the classic electrospinning, the whipping zone is absent. The typical tip–collector distance is in the range 0.5–3 mm [89]. Because of such a close distance, the required electrostatic voltage is reduced [90], maintaining anyway the typical value of the electrical field in the region (about 10^7 V/m) [89]. With this process single, thin (even less than 100 nm diameter) and several centimetres long nanofibers can be obtained [90,91]. The fibers are deposited in a similar way of the 3D printing and moving the collector with adequate speed allows to draw the fibers in a controllable manner [92]. The morphology of the fibers can be tuned changing the solution concentration, the electrode-collector distance, the applied voltage, the tip diameter, the size of the droplet [89,90,92]. The environmental parameters are the same of the conventional electrospinning listed above.

3.2. Chemical vapour deposition

The chemical vapour deposition (CVD) is a synthesis technique used to obtain a solid support from a molecular precursor (Fig. 3D). It consists in the thermal decomposition of a hydrocarbon vapor in presence of a metal catalyst. It is the most employed methodology to produce carbon nanotubes (CNTs), that are carbon-based nanostructured tubular elements. Since mid-twentieth century, CVD is an established method for microfibers production and in 1952 researchers obtained 50-100 nm diameter CNTs. The CVD for CNTs manufacturing consists in a hydrocarbon vapor flowing through a cylindrical reactor, in which a metal catalyst is present. The catalyst, heated at a proper temperature (600-1200°C), decomposes the hydrocarbon from the vapor into carbon and hydrogen species. Hydrogen flies away and carbon gets dissolved into the metal [93]. Once the solubility threshold of the carbon in the metal is reached, it precipitates and crystallizes in a network-shaped structure energetically stable, the CNT. Upon cooling the system, the CNTs are collected. However, the CNT growth mechanism is still not well known [93]. The CVD is widely used because of its reasonable processing cost, high production yield, the ability to control the crystal structure and the deposition rate [94]. Many parameters can be set to tune the CNTs structure: the hydrocarbon type, the catalyst, the temperature, the pressure, the gas-flow rate, the deposition time and the reactor geometry [93].

4. Materials employed in muscle-inspired fibers production

In order to produce fibrous actuators, different materials with specific peculiarities had been used. A class of materials frequently employed is represented by conjugated polymers: organic semiconductors characterized by single or double bonds alternated along the polymeric backbone [59]. This configuration confers them electrical conductivity: once an anion approaches the chain, it forces the polymer to reconfigure itself, sliding its double bonds along the chain. This creates a flux of electrons and, consequently, an electronic current. Applying a potential to the polymer ends, a volumetric change occurs, a phenomenon mainly caused by mass transport. The applied potential creates a charge mismatch, balanced by the entrance of anions or cations (often solvated) into the interstices of the polymeric chain. The polymer thus contracts or expands by changing its volume. Polyaniline, polyacrylonitrile, polypyrrole and poly(3,4ethylenedioxythiophene) belong to this class. These materials can be used both as electro-active coating and to produce fibers themselves.

Carbon is also frequently used. Specifically, CNTs are a class of allotropes of carbon with cylindrical nanostructure. They have appealing properties like low density, high tensile strength, high conductors of electricity and/or heat. CNTs are often obtained in form of multi walled carbon nanotubes (MWCNT), consisting in several concentric graphene tubes [95]. They can be grouped in yarns and twisted to make spring-shaped structures able to contract axially and to rotate in response of various kind of stimuli [96–98].

The same principle is shared with some non-conductive polymers or natural fibers that, when over-twisted, rely on their anisotropic thermal expansion coefficients to produce actuation [98]. Other passive fibers, like silk, can be used as bulk materials to produce nanofibers. These fibers are often responsive to humidity changes, making them suitable for soft-actuators production [99]. Other materials, usually conjugated polymers, are frequently used as coating on the fibers, to achieve a response to the stimuli [100]. Recently, molecular motors (MM) had been developed starting directly with the artificial assembly of a molecule capable to change its length in response to a stimulus [101–105] (Tables 2 and 3).

5. Analysis of state-of-the-art of muscle-inspired actuators

In this Section, the state-of-the-art of muscle-inspired actuators is analysed. Specifically, the literature will be classified considering the hierarchical level reached and tested, i.e. single fibers, flat mats, bundles, yarns, coiled and/or plied structures (Table 4).

5.1. Single fiber actuators

Up to now, only a few works involved actuators made of individual fibers. In [113], hydrogel nanofibers had been produced through the electrospinning technique. The main aim of the work was to investigate the actuation performance of a single hydrogel nanofiber made of PAA. The atomic force microscope (AFM) was used to measure forces in the nanonewton scale [131]. The PAA nanofibers were directly electrospun across two parallel 40 μm thick bars of a transmission electron microscopy (TEM) stub, 50 μm spaced from each other (Fig. 4).

After an ultra-violet light (UV) crosslinking the fiber was mechanically tested hooking the AFM cantilever tip transversely to its axial direction. In a first test, the nanofibers were deposited slack across the bars (Fig. 4AI) and later activated by pH variations of the bathing solution. Moving from pH 8 to 3, a swelling of the nanofiber was observed, with a consequent axial contraction (response time = 1-4 s) until its complete stretching between the bars (Fig. 4AII). In a second test, the nanofibers were pre-stretched with a constant strain by the cantilever tip movement. With a series of tip oscillation and pH variations, the nanofibers mechanical properties were determined: a 20–24% axial strain was reported during the free stroke in the first test, while during the second one (comparable to an isometric contraction) an elastic modulus of 8.5 MPa (pH=3) and of 5.1 MPa (pH=8) was determined. The contractile force was 0.5 μN, corresponding to a mean stress of 230 kPa, comparable to skeletal muscles [30,47].

In [132], the NFES technique had been used to produce PVDF fibers (diameter = 2.6 μm, length = 500 μm) studying their individual actuation (Fig. 4B). The PVDF fibers were spun across two aluminium contact pads suspended over an insulating glass

Table 2
Materials used to produce muscle-inspired actuators

Acronym	Extended Name	Manufacturing technique	References
PANi	Polyaniline	Electrospinning	[4,61,106]
PAN	Polyacrylonitrile	Electrospinning	[107,108]
CNT	Carbon Nanotube	Chemical Vapour Deposition	[12,14,60,109]
PPy	Polypyrrole	Coating	[65,100]
PEDOT	Poly(3,4ethylenedioxythiophene)	Coating	[65,100,110]
PES	Polyester	-	[65]
-	Nylon 6.6	Dry / wet / Melt spinning	[111]
-	Silk	Electrospinning Natural harvesting	[100]
PVDF	Polyvinylidene fluoride	Electrospinning	[112]
MM	Molecular Motors	Solvent Casting	[105]
PAA	Polyacrylic acid	Electrospinning	[113]
-	Cellulose	Electrospinning	[106,112,114]
PET	Polyethylene	Melt Spinning	[10,115,116]
PU	Polyurethane	Electrospinning	[61]
ZrO_2	Zirconia	Electrospinning	[117]
-	Spandex	Melt Spinning	[118]
UHMWPE	Ultra-molecular weight polyethylene	Melt Spinning	[116]
GO	Graphene Oxide	Wet spinning	[119]
Nb	Niobium	Etching	[9]
PEVA	Poly(ethylene-co-vinyl-acetate)	Melt Spinning	[120]
-	Wool	Natural harvesting	[121]
-	Cotton	Natural harvesting	[121]
-	Flax	Natural harvesting	[121]
-	Cotton	Natural harvesting	[122]
-	Viscose	Melt Spinning	[123]

Table 3
Coating, electrolytes, and additives used to enhance muscle-inspired actuators contraction

Acronym	Extended Name	Usage	References
PANi	Polyaniline	Coating / Particles inclusion	[4,61,106]
PPy	Polypyrrole	Coating	[61,100,124]
MWCNT	Multi Walled Carbon Nanotubes sheet	Coating	[111]
PEDOT	Poly(3,4ethylenedioxythiophene)	Coating	[65,100]
-	Graphene	Coating	[125]
Pt	Platinum	Coating	[126]
Ag	Silver	Coating	[10,65]
Au	Gold	Coating	[65]
C	Carbon	Particles inclusion	[65]
Sn	Tin	Coating	[65]
Al	Aluminium	Coating	[120]
Cu	Copper	Coating	[65]
p-TSA	Para-toluene sulfonic acid	Coating	[100]
NaDBS	Dodecylbenzenesulfonate	Coating	[100]
-	Wax	CNT-structures guest material	[127]
PDDA	Poly(diallyl dimethylammonium chloride)	CNT-structures guest material	[128]
TPU	Thermoplastic Polyurethane	CNT-structures guest material	[96]
PVDF-co-HFP + TEA•BF4	Poly(vinylidene fluoride-co-hexafluoropropylene) + tetraethyl ammonium tetrafluoroborate	Gel electrolyte	[12,13]
PVA + H_2SO_4	Polyvinyl alcohol + Sulfuric acid	Gel electrolyte	[13]
TBA•PF_6	Tetrabutylammonium hexafluorophosphate	Organic electrolyte	[12,97,129]
PEO-SO_3	Sulfonated Poly(ethylene Oxide)	CNT-structures guest material	[130]
TBA•PF_6/PC	Tetrabutylammonium hexafluorophosphate + Propylene carbonate	Organic electrolyte	[130]

substrate, fixing their ends with conductive epoxy on the pads (Fig. 4BI). PVDF has a negative piezoelectric coefficient, so positive or negative electric fields cause respectively a shrinkage or elongation [132]. The suspended fibers showed an initial downward deformation due to gravity force, measured with a charge-coupled device (CCD) sensor as the variation of downward flexion in the central part of the fiber (Fig. 4BII). The authors reported a bias in the data caused by the electrostatic attraction of the fiber toward the pad. This side-effect was minimized by placing two identical electrodes symmetrically over the main ones (Fig. 4BIII). The PVDF electrospun fibers showed about a two-time higher piezoelectric coefficient compared to commercially available PVDF films. This coefficient is directly proportional to the induced mechanical strain. It was concluded that this improvement was due to the fewer defects and smaller domain wall motion barrier in the PVDF electrospun fibers.

Only a few works investigated the properties of single fibers mainly because of the challenging testing procedures according to the dimensions of the fibers and the infinitesimal forces to be measured (from nN to a few μN [113]).

5.2. Flat Mat actuators

Trying to obtain a scaled up hierarchical complexity of their actuators, other researchers focused on the production of fibrous mats. Preliminary works investigated commercially available wet and dry spun PAN fibers [126,133–135]. In [133], an artificial muscle made of PAN fibers was activated through an electric field. This activation was obtained bathing the structure in an aqueous solution of sodium chloride in contact with one of the two electrodes. The local acidity of the solution changed near the electrode, implying the contraction or expansion of the artificial muscle depend-

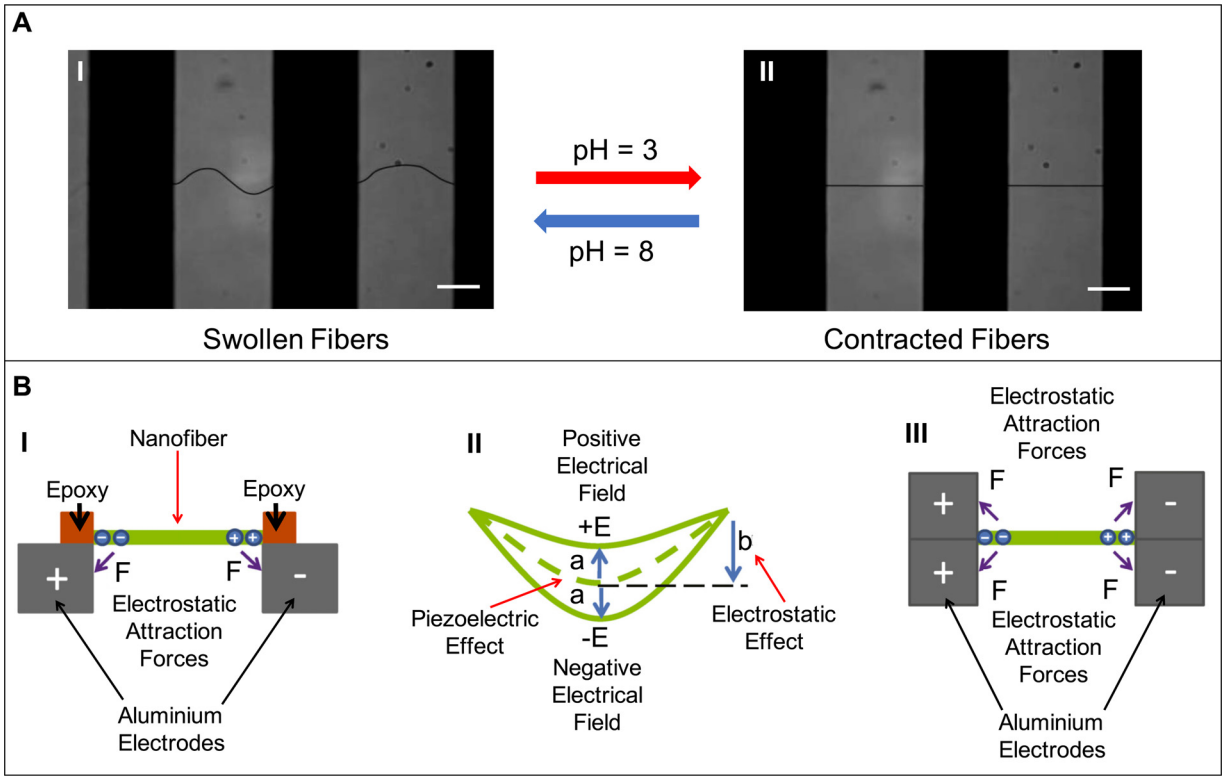

Fig. 4. Single fibers actuation. A) Optical microscope images of PAA nanofibers UV treated for 5 minutes and suspended between bars of a TEM grid at different pH values (adapted from [113] and reproduced with permission. Copyright 2012, The Royal Society of Chemistry): I) swollen fibers (pH = 8; scale bar = 20 μm); II) contracted fibers (pH = 3; scale bar = 20 μm). B) Piezoelectric actuation of PVDF nanofibers fixed between two aluminium contact pads (adapted from [132] and reproduced with permission. Copyright 2010, Elsevier B.V.): I) scheme of the electrostatic attraction forces between the nanofiber and aluminium pads; II) deformation of a PVDF fiber under positive (+E) or negative (−E) electrical field as a result of (a) piezoelectric and (b) electrostatic effects; III) adding two aluminium electrodes upside, the electrostatic force can be reduced.

ing on the polarity of the electric field. In a later study the authors added two steps of annealing and chemical treatment to the PAN fibers, reaching a 100% strain during the activation [134]. The force dominating the contraction-expansion of PAN fibers were reported to be mainly intermolecular Coulomb ones. Trying to increase their conductivity, the muscle-inspired PAN fibers had also been coated with platinum [126]. However, the contraction speed was quite low, reaching a 40% contraction in 10 minutes. To increase the ions/solvents diffusional processes that governs the PAN contraction, the contraction speed and the response time as well, the electrospinning technique was adopted to produce mats of PAN nanofibers [108]. The same investigation was carried on in [107,136], where the shape changes of PAN nanofibers in response to a pH variation had been observed. The changes of the nanofibers diameters were also measured *in-situ* with an environmental scanning electron microscope (E-SEM) and an AFM. A variation of more than 100% was observed [134] with an increase of the mean diameter of PAN nanofibers from 250 to 750 nm, after the contraction [107,136]. In [4], to improve the overall actuator performances, a biomimetic perspective was investigated, exploiting the nanoscale range and the higher molecular alignment within individual fibers to increase the Young's modulus [137,138]. Electrospun PAN nanofibers were collected in randomly aligned mats and then annealed. Several stripes of the PAN mat were cut and divided in three groups to be passively mechanically characterized in different states: annealed, fully contracted (in a low pH solution) and fully expanded (in a high pH solution). Each category showed different values of ultimate stress and strain (i) annealed samples 0.07 MPa at 8%; (ii) fully expanded 3.5 MPa at 42%; (iii) fully contracted 80 MPa at 125%. A composite actuator was then produced, embedding a graphite electrode sheet between two layers of electrospun PAN nanofibers. A 25% linear contraction in 1 minute was observed when electrically activated, with a maximum strain of 58.8%, an ultimate stress of 77.1 MPa, and a Young's modulus of 0.21 MPa [4].

Cellulose acetate combined with synthetic polymers is an alternative strategy when prototyping contractile flat mats of nanofibers. An electrospun cellulose acetate-polyaniline (PANi) biocomposite membrane was proposed as soft-actuator in [106], where the cellulose acetate fibers, embedded with chopped PANi particles, were directly electrospun. Just a low amount of this conductive polymer was sufficient to enhance the performance of this cellulose-based biopolymer actuators [106]. The obtained nanofibers were collected in randomly oriented mats and placed between thin gold electrodes. The devices were electromechanically tested with harmonic responses and current-voltage tests, showing an electrically driven bending deformation. The entity of the displacement was correlated with the amount of PANi inside the cellulose-acetate nanofiber [106]. The contraction was not linear probably due to the random arrangement of the nanofibers.

5.3. Bundle and yarn structured artificial muscles

Following the hierarchical structure exhibited by biological skeletal muscles, researchers investigated parallel (bundle) or twisted (yarn) fibrous topologies, to enhance the actuation performances. A bundle of 50 μm PET fibers, platinum coated, was produced through melt spinning [124]. The whole bundle was then coated with an additional layer of PPy. Since this kind of actuator needs a liquid electrolyte, the bundle shape was chosen to facilitate the ion diffusion kinetics and to decrease the electrical resistance, avoiding the limitations previously observed in PPy-film ac-

tuators [139]. The device weight fraction, constituted by the active component was then calculated, resulting in an increase from 0.3 of the double-sided laminated film (thickness = 100 μm; PPy coating thickness = 20 μm), to 0.64 of a bundle of PET platinum coated fibers that occupies the equivalent area of the film. The mechanical tests reported a maximum stress of 6.8 MPa.

Bundles of PAN microfibers, coated with conductive platinum, were produced in [140]. These bundles were used inside a chemical electrolytic cell as an electrode and activated with a 10 V DC power supply. A pH change in the vicinity of the PAN bundle electrode was then observed, leading to a contraction of up to 100% of the bundle within a few seconds.

In another study [65], the performances of seven different kinds of actuators, produced starting from commercial yarns, were evaluated: spun yarns (of polyamide, silicon or cellulose) with carbon particles inclusion; polyamide silver coated; polyester yarn wounded by a stainless-steel wire; polyester yarn double wounded by a copper wire; gold coated polyester yarn. Finally, all these yarns were coated with a conductive PPy layer. The actuation of the yarns showed a linear contraction in a range of 0.01 – 0.1% [65].

Other groups instead worked on the development of artificial muscles based on CNTs, which is one of the most prolific fields. Firstly, a novel method to obtain yarns of multiwalled carbon nanotubes (MWCNTs) was introduced, inserting a twist during their drawing from the, so called, nanotube forest [141] (Fig. 5AI - II). These yarns have shown to achieve ultimate stresses greater than 460 MPa with about 9% strain. In [142], MWCNTs were used to develop a soft actuator. The dependence of the actuation strain on the applied voltage were quantified. A linear strain of 0.5% was obtained in response to a 2.5 V electrical stimulus. This dependence was found to be quadratic, whereas the Young's modulus was independent from the applied load or voltage. A similar structure was proposed in [129], where a muscle-inspired electromechanical actuator was produced with a twisted CNT yarn, filled with an electrolyte (i.e. 0.2 M TBA•PF6 in acetonitrile). The yarn was firstly obtained by harvesting and twisting MWCNTs from a nanotube forest. Then it was put, together with a counter electrode, in the electrolyte bath with an applied voltage between the two electrodes. For the electrochemical double-layer charge injection, the yarn partially untwisted. The actuation performances showed a reversible maximum rotation of 41 full turns, corresponding to 3.4% of the twist inserted in the actuating yarn length. However, the linear maximum contraction was about 1%, far from the one observed in skeletal muscles (i.e. 20-40% during physiological activities [143,144]). A slightly better contraction was obtained in [145], by using left and right-handed fibrous yarns of similar twisted and aligned MWCNTs, (diameter = 20 μm) (Fig. 5AII). These assemblies were firstly actuated in air, obtaining reversible lengthwise contractions up to 2% and rotatory torsions larger than 360°. These results were equivalent for both left- and right-handed yarns. Their rotations and contractions were quite fast (< 0.4 s) and the developed stress reached 6 MPa during an isometric test onto a tabletop testing instrument.

In [127], a hybrid electrothermally powered MWCNTs yarn had been produced, by exploiting the same strategy that spiders use in Nature to eliminate uncontrolled spinning at the end of the dragline. To damp unwanted dynamic oscillations, the yarn was infiltrated with paraffin wax. Moreover, the wax, mixed with a triblock copolymer, was characterized by a large thermally induced volume change that can also enhance the yarn lengthwise contraction when activated [146]. In a later work, the conductivity of MWCNTs was increased by depositing graphene flakes on the MWCNTs sheets, during yarns production [125]. In this way, the conductivity of the device increased to 9×10^4 S/m (from the 22×10^4 S/m of the pristine MWCNTs).

As an alternative to CNTs, niobium nanowires were proposed as high strength yarn-based artificial muscles [9]. To extract highly aligned niobium nanowires, copper had been etched from copper-niobium wires (diameter = 100 nm). These filaments were later twisted into yarns of different diameters and electromechanically characterized. The devices showed strong values of ultimate strength (from 0.4 to 1.1 GPa), higher conductivity than CNTs (3×10^6 S/m versus 3×10^4 S/m) and mean tensile moduli of about 19 GPa. The electrical activation, with a pulse of 4.8 V, generated a maximum value of 1800 rpm, despite a tensile actuation of only 0.24%, even lower than CNTs actuators [142,145].

The electrospinning technique was also proposed as a suitable tool to produce bundles resembling the skeletal muscle myofibrils and myofibers. PU nanofibers coated with PANi were proposed in [61]. PU was chosen because of its rubbery and flexible nature in order to follow the contraction of PANi without blocking its actuation. An axially aligned bundle was obtained with a gap collector during the electrospinning process. The nanofibers were then coated with a 260 nm thick layer of PANi, using an *in-situ* chemical polymerization of aniline. The device was then tested with cyclic voltammetry, showing a high electroactivity. Current-voltage (I-V) plots were obtained, reporting 50 S/m of conductivity, that was considerably higher compared to the pure PU nanofibrous bundle (1.76×10^{-6} S/m). The electromechanical characterization revealed a linear contraction of 1.65% at an applied stress of 1.03 MPa. The bundle could stably be actuated without significant creep, at an applied stress up to 2.263 MPa (linear strain of about 0.6%). The work per cycle was reported with an efficiency above 75% during the actuation, even beyond 100 cycles. The device was also passively tested, reporting an ultimate strength of 35 MPa, higher than the ultimate strength of a pure PU nanofibrous bundle (25 MPa).

In [100], the electromechanical actuation of electrospun silk fiber bundles was proposed to mimic the muscle fiber. Silk fibroin was chosen due to its biocompatibility, as demonstrated in drug delivery [147] and tissue engineering of similar hierarchical biological structures [148]. Silk nanofibers were first electrospun on a high-speed rotating drum collector in an aligned pattern; mats were later rolled up directly on the drum (Fig. 5BI) to obtain bundles with an average diameter of 200-500 μm (Fig. 5BII - III), the same order of magnitude of muscle fibers. The fibers then underwent sequential chemical and electrochemical polymerization to increase the hydrophilicity of the fibers and the incorporation of the conductive polymer. These processes also changed the colour of the bundles (Fig. 5BII). Then, to form a silk-PPy interpenetrating network, a PPy deposition was carried on *in situ,* soaking the bundles in a polymerization solution containing PPy and $FeCl_3$. This step turned the bundles sufficiently conductive to be used as working electrodes for an additional conductive coating step, using p-TSA or NaDBS as dopants (or PEDOT as an alternative to PPy). The resulting nanofibers exhibited conductivities in the order of 10^3 S/m. Using a square wave of ±2 V to actuate the devices, the bundles coated with PPy and doped with p-TSA achieved a maximum stress of 400 kPa, in the same range of skeletal muscles. While devices employing PEDOT showed higher stresses and relaxation rates (0.12%/s), the PPy coated and doped with NaDBS showed the longest lifetime, being fully operational after 24 hours, but with a stress generation capacity dropped to a fifth of the initial value. However, the maximum strain was still low when compared to natural muscles, reaching maximum values of 1-2%.

In [105], a hierarchical self-assembly of photo-responsive amphiphilic MM [102,149–151] was proposed. This work relies on an unpreceded amplification of motion, starting from the molecular level over various length scales, up to a macroscopic contractile movement of a hierarchical fibrous structure [105]. Rotary MM were synthetized in such a way as they automatically self-assemble in a supramolecular unidirectional aligned system

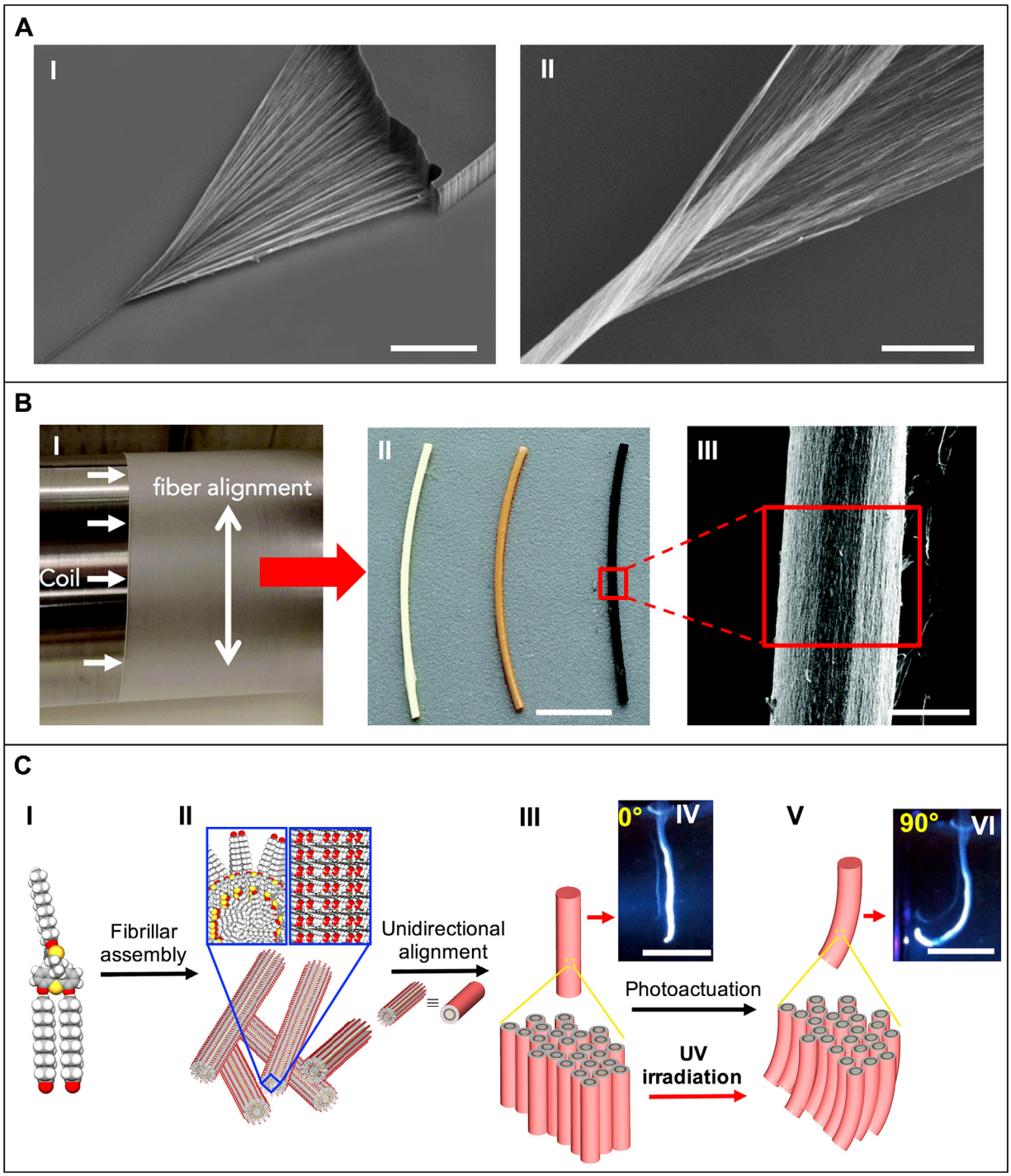

Fig. 5. Applications of fibrous bundles and yarns in the production of muscle-inspired soft-actuators. A) Scanning electron microscopy (SEM) image showing the production of a MWCNTs yarn obtained by twisting during drawing from a nanotube forest (adapted from [171], reproduced with permission. Copyright 2010, Elsevier B.V.): I) overview (scale bar = 500 μm); II) zoom into the carbon nanotube yarn (scale bar = 250 μm). B) Electrospun silk fibroin electromechanically actuated bundles (adapted from [100], reproduced with permission. Copyright 2017 The Royal Society of Chemistry): I) production by rolling up nanofibrous mats on a drum collector; II) different chemically treated bundles (scale bar = 50 μm); III) SEM image of a bundle cross-section (scale bar =200 μm). C) Nanofibrous bundle actuated by means of photo responsive MM (adapted from [105], reproduced with permission. Copyright 2017 Springer Nature): I) Picture of a photo responsive molecular machine; II) self-assembly of molecules into nanofibers; III) assembly of nanofibers in axially aligned bundles; IV) image of a bundle before the application of the UV light (axial alignment = 0°; scale bar = 5 mm); V) bundles nanofibers bending after the UV light application; VI) image of a bended bundle after the application of the UV light (radial bending = 90°; scale bar = 5 mm).

to form a nanofiber (Fig. 5CI). Then, the solution containing the MM was matched into an aqueous solution of calcium chloride ($CaCl_2$) with a pipette to automatically obtain a noodle-like bundle of aligned nanofibers (Fig. 5CII - IV). This string, about 10 mm long and comprising 95% of water, was activated with a light source that induced the rotation of the rotary MM and, thus, the bending of the string toward the light source (Fig. 5CIII – VI). The macroscopic bending of the string was caused by the orientational changes of the bundles [105]. A 90° string bending was obtained in water after 60 s of irradiation; to restore the string original conformation, it was necessary to heat the water for 3 hours. A similar test was carried on in air, with a 0.4 mg piece of paper attached to the end

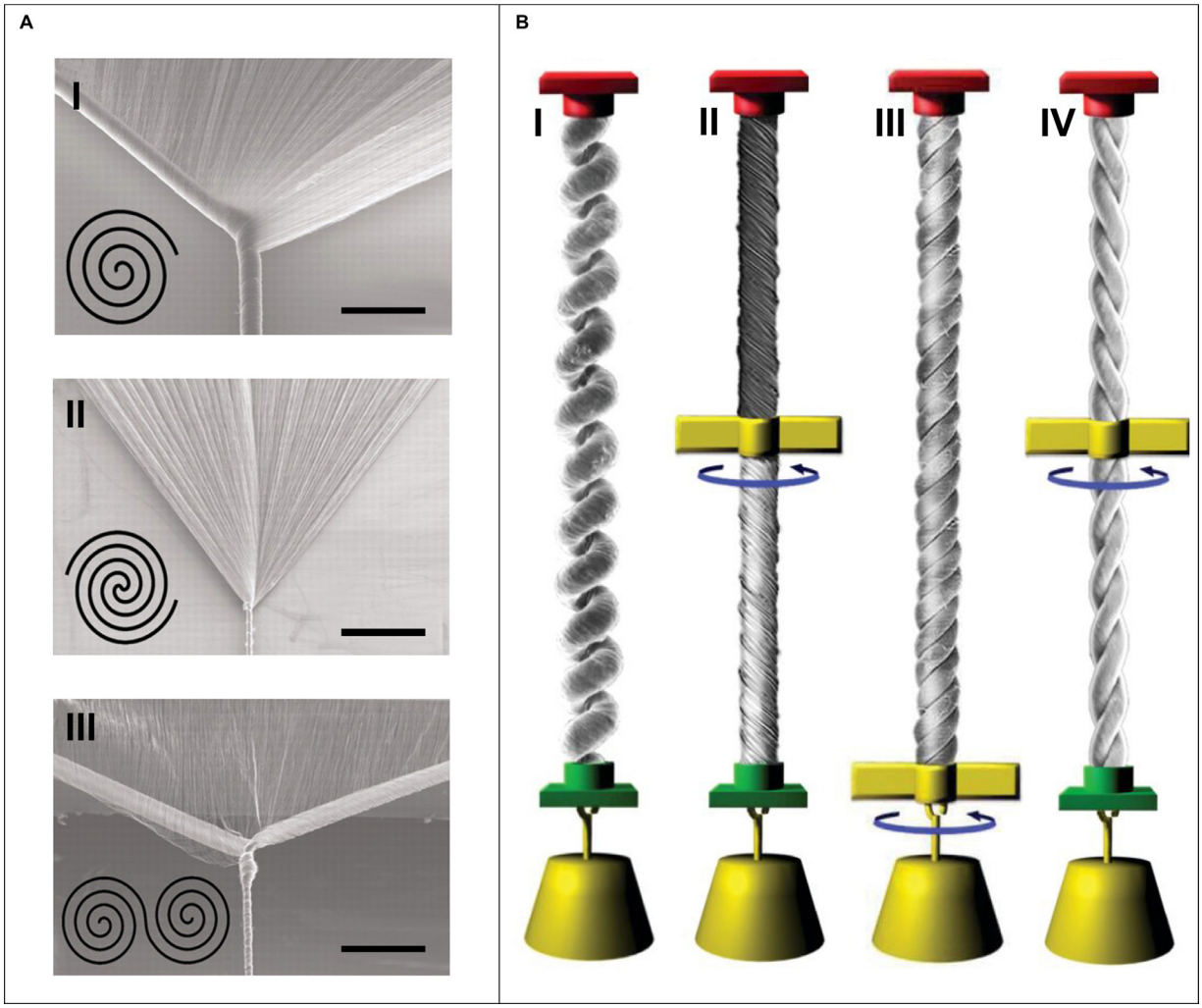

Fig. 6. Yarn configurations for linear and torsional actuators. A) Different methods of twist insertion during spinning of a MWCNT sheet. The cross section scheme of the yarn is shown in the inset (adapted [154], reproduced with permission. Copyright 2002 Science Magazine): I) Fermat-type twist insertion (scale bar = 75 μm); II) Archimedean-type twist insertion (scale bar = 250 μm); III) Dual-Archimedean-type twist insertion (scale bar = 300 μm). B) Different muscle configuration using twisting, coiling and plying techniques (adapted from [14], reproduced with permission. Copyright 2012 Science Magazine): I) two-end-tethered, fully coiled wax infiltrated homochiral muscle; II) two-end-tethered, half wax infiltrated, noncoiled homochiral muscle. A paddle, free to rotate, separates in the middle the infiltrated and the neat part of the device; III) one-end-tethered, fully wax infiltrated, 4-ply homochiral muscle; IV) two-end-tethered, fully wax infiltrated, 2-ply heterochiral muscle. The paddle, free to rotate, separates in the middle the two opposite-twisted part of the device. Red and green attachments are tethers that prohibit end rotation. Red ones prohibit also translational displacement.

of the string. After irradiation, the device was able to bend of 65° in 60 s, lifting the paper. Even if the proposed actuator involves a bending motion, which is far from one of the topics of this review, it is interesting to note that in this case the basic actuating units are the molecules themselves. These MM firstly self-assemble in aligned systems to form nanofibers and finally were grouped together producing a bundle-like hierarchical structure.

5.4. Coiled and/or plied structured artificial muscles

The amount of contractive strains and actuating forces is particularly critic for muscle-inspired actuators. To overcome these problems, researchers adopted techniques such as twisting, coiling, and plying [16,152]. A coiled structure is obtained by overtwisting a single yarn, while twisting several yarns together leads to a plied assembly. These types of actuators can produce force through torsional motion [153] or linear contraction. In this review, for the reasons presented above, only the studies belonging to the latter category will be described. In [14], a guest-filled MWCNT yarn actuator was designed. The need of an electrolyte (with a counter-electrode and a packaging) is another common drawback of these devices [129,142]. In [14], the actuating guest (i.e., paraffin wax) between MWCNTs was incorporated in both solid and molten state to avoid this limitation. The volume expansion of the wax drove the actuation (about 20%, while the temperature increases from 30°C to 90°C). Wax was not extruded from the porous yarn due to the high interfacial energies arising at the nanoscale [14]. This guest confinement inside the nanoscale pores of the MWCNT yarn was intended to avoid hydraulic and external heating systems. These hybrid yarns contained up to 99% in weight of the guest substance without losing the flexibility and the properties of the CNT host structure [13]. Furthermore, in [14], many different structures had been proposed, starting from the harvesting of the MWCNT sheets from the CNT forest. During the twist insertion of the sheets to form the yarn (Fig. 5AI), the paraffin wax was eventually inserted with the biscrolling technique. To incorporate the wax into the yarns, the sheets were twisted in different-shaped structures depending on the desired application [14]. The typical yarn-guest structures are known as Fermat, Archimedean and dual-Archimedean scrolls and originates by the twist movement that is imparted to the sheets during the yarn production [154] (Fig. 6AI-III). Furthermore, homochiral and heterochiral structures had been

proposed (Fig. 6BI-IV) [14]. The latter were obtained by inserting a paddle in the middle of the yarns: in this way, one half was twisted in the opposite direction of the second half. A coiled dual-Archimedean neat (without wax) yarn was firstly tested by heating, showing a 7.3% contraction under 3.8 MPa of applied stress. The contractile work capability (scaled on the yarn weight) was 0.16 kJ/kg. A two-end-tethered coiled Fermat wax-filled yarn was thermoelectrically activated with a square wave stimulus of 18.3 V/cm at 20 Hz. The devices showed for 1.4 million cycles a tensile contraction of 3% at a rate of 1200 cycles/minute, lifting 17700 times their own weight. A fast passive cooling of 25 ms was necessary between cycles. The same device was then optimized by increasing the electrical stimulation at 32 V/cm, reaching the capability to lift 175000 times its own weight, a contractile work of 0.836 kJ/kg, and a power output of 27.9 kW/kg, which was 85 times the peak value for mammalian skeletal muscles (0.323 kW/kg). As a drawback, a decreased life cycle of the device had been reported. To optimize the level of coiling of the actuators, an investigation was carried on yarns having different levels of inserted twists [14]. A coiled Fermat yarn with an intermediate twist (3990 turns/minute) showed a maximum contraction of 5.6% was observed with a 5.7 MPa of applied stress. Increasing the twist insertion by 6.8% (4263 turns/minute) resulted also in an increment of the maximum contraction (16.4 MPa at 5.1% strain) and of the contractile work (1.36 kJ/kg at 84 MPa). Conversely, the reduction of the twist insertion by 41% eliminated the coiling, thus reducing the maximum contraction at 0.7% and the contractile work to 0.31 kJ/kg. A partially coiled dual-Archimedean yarn produced a 10% of contraction at 5.5 MPa of applied stress. This improvement was achieved by increasing the yarn diameter of about 13 times; as drawbacks the cooling time increased to 2.5 s and, thus, the contractile power lowered to 0.12 kW/kg. A two-handed-tethered homochiral Fermat yarn, half wax impregnated and half not (separated in the middle by a pad) was also tested. When thermoelectrically activated, the actuator was able to rotate the paddle at 11500 rpm, first in one direction then in reverse. The device showed a high life cycle, due to the simultaneous twisting of the unactuated half during the untwisting of the actuating half (the unactuated half acted as a torsional return spring [127]) (Fig. 6BIV). Furthermore, the same work showed how the wax infiltration and the coiling increased the tensile contraction of yarns as well as how the reversibility of the actuation was greatly enhanced by having a sufficient twist to cause coiling [14].

A similar guest-filled hybrid CNT torsional and linear yarns were proposed in [13]. The peculiarity of these actuators was the solid gel electrolyte (PVDF-*co*-HFP based TEA•BF_4) in which they were embedded. These actuators were electrochemically driven, a method used to increase the efficiency compared to electrothermal activation [13]. A MWCNT sheet was pulled from a forest and a twist was inserted to produce yarns with a high oriented fibrous structure (Fig. 7AI and II). To produce torsional actuators, two yarns were firstly embedded in the gel electrolyte and, subsequently, were plied together in a two-ply (2-ply) mechanically coupled assembly, using opposite directions of twist (Fig. 7AIII). The two yarns were then used as anode and cathode. A square-wave stimulation of 2.5 to 5 V resulted in a reversible torsional stroke of 14-53°/mm with a minor hysteresis. Conversely, the linear actuators were obtained using two fully coiled yarns (Fig. 7AIV). These two coiled yarns (i.e., anode and cathode) were simultaneously infiltrated and coated with an aqueous solid gel electrolyte (PVA in sulfuric acid) and plied together in a 2-ply artificial muscle (Fig. 7AV). A linear contraction of 0.52% was obtained, applying a square wave of 1V (at an applied stress of 11 MPa). Other trials in the same work [13] obtained 1.3% contraction at 10.1 MPa with a stimulation of 2.5 V. While it was quite fast (about 1 s) to obtain the first 1% of contraction, the stimulation needed to achieve its maximum contraction was quite longer (about 20 s). Unlike the electrothermally powered artificial muscles, these devices did not require any further energy input to maintain the contraction.

Another actuation method, with solvents and vapours, was employed in [109] to drive helical CNTs artificial muscles (Fig. 7B). Using the dry-spinning technique, MWCNTs were drawn from a forest to form a yarn (named primary fiber; diameter = 15 μm) (Fig. 7BI). Twenty yarns were then plied together in a 2-levels hierarchical structure (Fig. 7BII)., later over-twisted to became fully coiled (3-levels hierarchical structure) (Fig. 7BIII). These structures were made with different helical angles: 0°, 8°,16°, and 32°, using a left-handed twisting. The 3-levels structures were then exposed to a polar solvent, an ethanol droplet, showing a rapid reversible contraction (about 0.5 s) able to last for 30 cycles (Fig. 7BIV and VI). The contractive peak stress of 1.5 MPa was reached with the 32° helical angle 3- levels structures. This actuator rotated at 6361 rpm, resulting capable of 738 turns/mm of the muscle length. The maximum linear contraction was about 10%. The total work density calculated, including rotatory and contraction outputs, was 26.7 J/kg. The response rate was further investigated, reporting a contractive strain rate of 340%/s [109]. The 2-levels structure was also tested (without coiling) using the ethanol droplet, showing an excessive irreversible untwisting, confirming that the coiling process enhanced the reversibility of the actuation (Fig. 7BIV andV). The 3-levels structure, instead, was shaped into a spring with a left-handed chirality, showing up to a contraction of 59% when activated through the narrowing to a liquid surface of dichloromethane (Fig. 7BVII to 7BIX). Finally, many 3-levels structures were woven in a net that, when sprayed with ethanol, was capable to lift a ball 100 times heavier than the net itself for 4.5 mm within milliseconds. For comparison, a single-ply helical fiber (SHF) actuator was produced over-twisting (plying) directly 20 layers of MWCNT sheets [109]. Even if the generated stress, once activated with ethanol, was similar to the 3-level structure, the stress rate was three times lower and the efficiency of the actuator markedly decreased after 15 cycles due to partial untwisting of the coils. The rotation speed was of 760 rpm, with 223 turns/mm of the muscle length. The responsiveness and the strain rate were 6.7 and 11.3 slower than the 3-levels structure. These differences were explained with the higher capacity of the solvent to infiltrate in the microscale gaps in the 3-levels structure, which were absent in the SHF actuators. Both types instead showed nanoscale gaps between CNTs [109].

In a later study, a 2-ply structure (Fig. 7CI and II) was infiltrated by an organic electrolyte (TBA•PF_6 dissolved in propylene carbonate) [12]. When activated with a pulse of -3.5 V (20 s long), repeated every 40 s, the obtained contraction was 16.5% (Fig. 7CIII) (maximum work density = 2.2KJ/Kg). Moreover, to avoid their immersion in an electrolyte bath, two parallel identical 2-ply coiled cathode-anode yarns were coated with a gel electrolyte made of TEA•BF_4 in PVDF-*co*-HFP (Fig. 7CIV and V). Actuating this device, the maximum contraction (11.6%) was obtained with an applied stress ranging from 12 to 30 MPa. The maximum work density was 1.12 kJ/kg, obtained at 45 MPa. Finally, to increase the hierarchical complexity, an all-solid-state artificial muscle with a braided core anode and a braided sheath cathode, both woven using four strands of the 2-ply coiled yarns, was fabricated (Fig. 7CVI) [12]. The anode and cathode were then embedded in a gel electrolyte (PVDF-*co*-HFP containing TEA•BF_4). When driven by a square wave of 5V at 0.1Hz square wave, the muscle showed a 5% contraction with an applied stress of 24 MPa. Since the contraction was partially inhibited by the coils contact, the tensile contraction increased with the load until the coil were separated [12]. In order to analyse the mechanical behaviour of the hierarchical helical actuators, a theoretical model, focused on the CNTs, was proposed in [155]. The properties of a two-level multi-ply CNT structure were

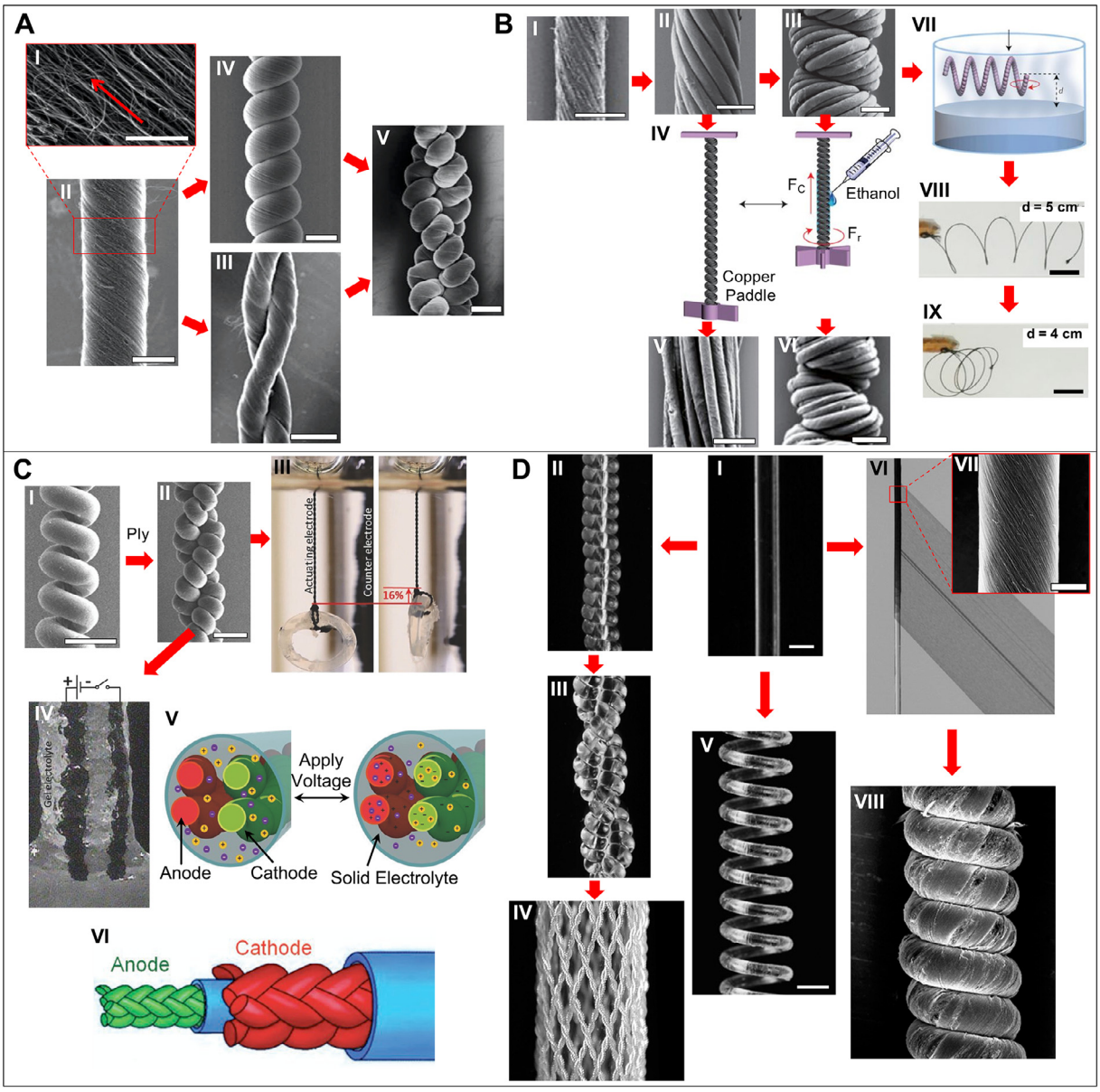

Fig. 7. Muscle-inspired plied and coiled soft-actuators. A) SEM images of different hierarchical assemblies (adapted with permission from [13], Copyright 2014, American Chemical Society): I) aligned CNTs on a yarn surface (scale bar = 1 μm); II) CNTs yarn of twisted nanofibers (scale bar = 20 μm); III) two twisted CNTs yarns (2-ply yarn) (scale bar = 60 μm); IV) single ply coiled CNTs yarn (scale bar = 60 μm); V) 2-ply coiled CNTs yarns (scale bar = 100 μm). B) Different applications of CNTs twisted and plied yarns soft-actuators (adapted from [109], images reproduced with permission. Copyright 2015, Springer Nature): I) CNTs yarn of aligned nanofibers (scale bar = 10 μm); II) twenty CNTs yarns twisted together (scale bar = 30 μm) until the over twist causes III) coiling (scale bar = 30 μm); IV) scheme of the contractive and rotary actuations of twisted or plied CNTs yarns. A copper paddle with a mass fixed at the end of the assemblies generated contractive and rotary forces simultaneously, when in contact with the solvent. V) The Twenty yarns twisted together in II) are progressively aligned by the contact with the solvent (scale bar = 40 μm); VI) the coiled structure in III) appears tightened by the contact with the solvent (scale bar = 100 μm); VII) schematic representation of a plied CNTs spring interacting at a distance (d) with a solvent; VIII) progressively self-contraction of the plied spring at a distance d = 5 cm and IX) d = 4 cm (scale bars = 2 cm). C) Electrochemically actuated CNTs muscle-inspired structures (adapted from [12], reproduced with permission. Copyright 2017, John Wiley and Sons): I) coiled CNTs yarn (scale bar = 200 μm); II) 2-ply CNTs yarn (scale bar = 500 μm); III) assembly actuation and shortening when immersed in liquid; IV) parallel pair of 2-ply coiled yarn coated with a solid gel electrolyte; V) cross-sectional schematics of the actuation mechanism of a 2-ply coiled all-solid-state actuator; VI) example of a braided muscle made from four 2-ply coiled yarns (red = cathode, green = anode, blue = gel electrolyte). D) Fishing line-based artificial Nylon 6,6 muscles (adapted from [111], images reproduced with permission. Copyright 2014, The American Association for the Advancement of Science): I) optical microscope images of a fiber (scale bar = 300 μm); II) the fiber after coiling by over twist insertion; III) a two-ply muscle formed from the coil; IV) a hierarchical textile braid formed from several two-ply, coiled, fibers; V) a coil formed by inserting twist in a fiber thermally annealed (scale bar = 1.5 mm) and coiling it around a mandrel; VI) helically wrapping a fiber with a forest-drawn CNTs sheet; VII) SEM images of a CNTs-wrapped fiber (scale bar = 75 μm) before and VIII) after coiling by twist insertion.

modelled to compare it with its bundle counterpart, concluding that the mechanical behaviour of the two-level structure can be controlled tuning features such as the CNTs handedness, number and initial helical angle of its plies.

A hybrid CNT-guest artificial muscle was designed in [128], using humidity changes or contact with water as actuation principles. MWCNT sheets were drawn from a nanotube forest and then immersed in the guest substance PDDA. After withdrawal from the solution, the sheets were twisted to form a wrinkled yarn, with 3700 turn/m of inserted twist, and then coiled. Upon activation, the yarn undergoes dimensional changes (like increased diameter, linear contraction and yarn untwist), enhanced by the guest sub-

stance [156]. The linear contraction capacity of this muscle resulted insensitive to both the water pH and temperature but depended on the applied stress. The authors obtained a 14.3% of contraction with an applied isobaric stress of 22.5 MPa, and a work capacity of 2.17 kJ/kg with a strain rate of 3.95%/s. At 0.54 MPa of applied stress the contraction reached 78%. When increasing the muscle diameter from 50 to 150 μm, using 21 MPa of applied stress, the yarns kept almost the same contraction (about 15%) and work capacity (about 1.9 kJ/kg) but decreased the strain rate (0.46%/s).

In general, during the actuation of twisted/coiled CNTs muscles, it is challenging to measure separately "but simultaneously" the linear strain along the yarn and the diameter change. To overcome this lack (and to better understand the whole actuation dynamic) an experimental setup was proposed in [157], employing a laser scan micrometer for a real-time data collection. In this work, two different artificial muscles were prepared: a neat CNT yarn obtained with a direct twist insertion on MWCNT sheets, and a hybrid CNT yarn with paraffin wax as guest material. When actuated, the system was able to measure a marked diameter change (about 10%) and a low axial strain (0.3%) for the neat yarn, while a minor diameter change (4%) and an improved axial strain (up to 2%) for the hybrid one.

CNT composite yarn-based muscles were investigated by electrothermal activation in [96], in which TPU had been used as guest material. A continuous CNT yarn was harvested by twisting MWCNTs from a nanotube forest and later immersed in a TPU/Dimethylformamide solution (i.e. 15% wt) for one hour. Four yarns were then plied together obtaining a 4-ply assembly. These structures were over-twisted into coiled yarns, annealed (with the two ends tethered) at 120° in a vacuum oven and subjected to several contraction cycles as training, to enhance their strain and recover ability. Once electrically activated, a maximum contraction of 13.8% in 5 s was obtained. The maximum contraction was achieved with an applied stress of 3 MPa, which resulted in a specific work capacity of 78.6 J/kg. Conversely, the maximum contractive stress achieved was 33 MPa, during a contraction of 3.6%, showing also a maximum work capacity of 547 J/kg [96].

A tethering-free twist-stable production method for CNT yarn had been proposed in [11]. Tensional tethering is generally needed to avoid excessive untwist of the muscle structures. Firstly, the authors prepared a CNT yarn from MWCNT sheets and over-twisted it into a fully coiled structure. The two ends were fixed closely to form a u-shaped yarn and a weight was hung in its central part: in this way, the yarn self-plied into a twist-stable double-plied yarn. Moreover, this process maximized the linear strain lowering near to zero the torsional stroke. When chemically activated with a droplet of acetone, the muscle showed a maximum contraction of 13.3% at an applied stress of 4.8 MPa with almost null rotation. The first 7% of contraction was obtained in 0.5 s and, to reach a contraction of 13.3%, it took additional 4 s (restoring time = 5.5 s). With an applied stress of 2.24 MPa, the contraction fell to 0.15%. The applied stress separated the coils making space for contraction that was, at low stresses, almost impaired. The maximum specific work of 847.2 J/kg was obtained at an applied stress of 9 MPa (about 8% contraction) [11].

In order to overcome drawbacks of the CNT guest filled yarn actuators, like the expensiveness and the difficulty to be activated in their entire volume, a sheath-run artificial muscle was proposed [130]. The authors developed a muscle in which the guest that drives the actuation is composed by a polymeric sheath that surrounds a twisted or coiled core. The goal was to avoid the reduced mechanical power output, caused by the limited chemical and transport times to access the volume of the yarn. CNT cores were employed to design linear actuators, coating them with a PEO-SO_3 or PU sheath. Upon activation, triggered by ethanol absorption, the actuator with PEO-SO_3 sheath showed a maximum contraction of about 15% at an applied stress of 33 MPa, and a maximum work capacity of 2 J/g at an applied stress of 65Mpa. The actuators with the PU sheath were electrothermally activated, showing about 13% of contraction at 42 MPa of applied stress. The maximum power density reported was about 1.35 J/g at 55MPa. To demonstrate the possibility to replace the CNT yarns of the core with an inexpensive material, commercial Nylon 6,6 fibers were employed in a form of coiled bundle, covered with a CNT sheath. This structure was electrochemically activated in a 0.2 M TBA•PF6 /PC electrolyte, reporting up to a 20% of contraction at 10 MPa of applied stress and a maximum 2.3 J/g work capacity at about 50 MPa.

Some works also proposed a new concept of inexpensive high-strength artificial muscles, usually referred as twisted and coiled polymers (TCP) muscles, obtained from twist insertion of polymer fibers used for fishing line or sewing thread [111,158,159]. In [111], commercially available PET and Nylon 6,6 microfibers were used, usually obtained through a melt spinning [160]. These fibers showed a large volumetric thermal expansion and anisotropy, caused by the flexible and highly oriented polymer chains, achieved during the spinning process [111]. Starting from Nylon 6,6 fibers (Fig. 7DI), an over twist was applied to obtain a fully coiled structure (Fig. 7DII). Once activated, to let the muscles contract, a load was needed to firstly separate the coils, which came in contact each other during the full coiling process. Moreover, to avoid untwist, two of these yarns were plied together (Fig. 7DIII). These Nylon 6,6 artificial muscles were activated by heating them from 20° to 240°C. Keeping a static load of 7.5 MPa, the coiled Nylon 6,6 actuators reached a contraction of 17% at 130°C. Then the adjacent coils touched and, with further heating, the muscle began to slowly elongate. The structure also showed a steep stiffening upon the coils contact, suggesting the possibility to obtain tuneable-stiffness muscles [111]. In order to maximize the muscle contraction, the authors also investigated the lowest applied stress to prevent inter-coil contact, showing a 22% of contraction at 22 MPa of applied stress. A 1.55 mm diameter coil was also proposed, made by inserting a twist in a Nylon 6,6 fiber (Fig. 7DI) and coiling it around a mandrel, with a final thermal annealing (Fig. 7DV). Once activated, this structure showed a 49% of contraction with 1 MPa of applied stress. A braid (Fig. 7DIV), made from 32 two-ply coiled Nylon 6,6 yarns, was used as a sheath of a heating element, delivering a 16.4% of contraction once heated, capable to lift a load of 630 g. In order to study the electrothermal activation, a conductive MWCNT sheet was wrapped around a Nylon 6,6 fiber (Fig. 7DVI-VII) that was later coiled (Fig. 7DVIII). This device was able to produce a contraction of 10% with a 22 MPa applied load. In the same work, PET muscles were also investigated, reaching lower contractions (up to 16%) due to the inferior melting temperature. However, PET coiled structures showed higher modulus and strength compared to Nylon 6,6 ones, making PET actuators suitable for lifting heavy loads with increased energy efficiency [111].

Later, the same polymer was employed to realize surface-modified twisted and coiled artificial muscles [10]. A PET fiber was twisted and coiled using a rotating applied load, then thermally annealed and trained using a different load. Finally, the assemblies were subjected to 10 heating-cooling cycles. Once thermally activated, the maximum contraction was investigated at different loading conditions, showing a maximum contraction of 8.6% with 500 g of applied load. Then, in the same work, another actuator using surface-modified PET fibers was proposed [10]: the PET yarn actuator, previously described, underwent a silver coating process to form an electrically conductive layer. The device was then activated through Joule heating, achieving a maximum contraction of 12.1% at 6V of applied voltage.

In order to introduce a strain self-sensing ability within a TCP actuator, in [161] the authors integrated a stretchable optomechanical film sensor into a TCP actuator based on Nylon 6.6 and Ag commercial fibers. Once activated by electrical stimulation, the actuator contraction gradually increases, leading to a colorimetric change of the sensor. The maximum contraction (33.3%) was achieved at 80 mA, with a developed force of 1.39 N.

Chemically cross-linked PEVA, a shape memory polymer (SMP), was also chosen to realize a coiled artificial muscle [120]. PEVA was melt extruded to form a precursor microfiber that was later wrapped by a Teflon tape and then by an aluminium foil. The PEVA-wire so obtained was then over-twisted to form a coiled artificial muscle. This structure and the neat straight PEVA microfiber were tested at the constant applied stress of 0.38 MPa and 0.55 MPa respectively, both activated by heating them from 20°C to 70°C. The neat PEVA fiber showed a maximum contraction of 19%, whereas the coiled structure 68%.

In another work the researchers investigated a twisted and coiled tensile actuator made of GO-based fibers with infiltrated Nylon 6,6 polymer, obtained with wet spinning [119]. The tensile actuation was driven by a volume expansion of the Nylon 6,6 once heated, whereas GO maintained a structural integrity at temperatures over the melting point of Nylon 6,6. The authors proposed both reversible contracting and elongating actuators, depending on the chirality imparted to the coiled GO-Nylon yarns (homochiral for contraction and heterochiral for elongation). When heated from

Table 4
Structure, activation type, mechanical performances, and materials of reviewed artificial muscles.

Structure	Activation	Maximum achieved Stress	Maximum achieved contraction	Main Material	Coating/additive/Guest material	Reference
Single Fiber	Chemical	230 kPa	24 %	PAA	-	[131]
	Piezoelectrical	-	-	PVDF	-	[132]
Flat Mat	Electrical	-	25 %	PAN	-	[4]
	Electrical	-	-	Cellulose	PANi particles	[106]
	Chemical	-	100 %	PAN	-	[134]
	Chemical	-	100 %	PAN	-	[107,136]
Bundle	Electrical	2.26 MPa	1.65 %	PU	PANi	[61]
	Electrical	400 kPa	2 %	Silk	PPy + p-TSA PPy + NaDBS PEDOT + NaDBS	[100]
	Electrical	6.8 MPa	-	PET - Pt	PPy	[139]
	Electrical	-	100 %	PAN	PANi - PPy	[126,140]
	Light	-	-	Molecular motors	-	[105]
Yarn	Electrical	-	0.01 %	PA + C	PPy	[65]
	Electrical	-	0.12 %	Silicon + C	PPy	[65]
	Electrical	-	0.05 %	PA	Ag + PPy	[65]
	Electrical	-	0.06 %	Cellulose + C	PPy	[65]
	Electrical	-	0.05 %	PES + Inox	PPy	[65]
	Electrical	-	0.03 %	PES + Cu/Sn	PPy	[65]
	Electrical	-	0.02 %	PES	Au + PPy	[65]
	Electrical	-	0.5 %	MWCNTs	-	[142]
	Electrical	-	1 %	MWCNTs	-	[129]
	Electrical	6 MPa	2 %	MWCNTs	-	[145]
	Electrical	-	-	MWCNTs	Paraffin Wax	[127]
	Electrical	-	-	MWCNTs	Paraffin Wax	[146]
	Electrical	-	-	MWCNTs	GO	[125]
	Electrical	-	0.24 %	Nb	-	[9]
Coiled/Plied	Electrical	84 MPa	7.3 %	MWCNTs	Paraffin Wax	[14]
	Electrical	11 MPa	1.3 %	MWCNTs	PVDF-*co*-HFP based TEA•BF_4	[13]
	Electrical	-	16.5 %	MWCNTs	TBA•PF_6 in propylene carbonate	[12]
	Electrical	45 MPa	11.6 %	MWCNTs	TEA•BF_4 in PVDF-*co*-HFP	[12]
	Electrical	24 MPa	5 %	MWCNTs	TEA•BF_4 in PVDF-*co*-HFP	[12]
	Electrical	33 MPa	13.8 %	MWCNTs	TPU	[96]
	Electrical	22 Mpa	10 %	Nylon 6,6	MWCNTs	[111]
	Electrical	-	33.3 %	Nylon 6,6 + Ag	-	[161]
	Electrical	50 MPa	20 %	Nylon 6,6	MWCNTs	[130]
	Electrical	-	44.1%	Nylon 6,6 + SMA	-	[162]
	Chemical	1.5 MPa	59 %	MWCNTs	-	[60,109]
	Chemical	22.5 MPa	78 %	MWCNTs	PDDA	[128]
	Chemical	-	2 %	MWCNTs	Paraffin Wax	[157]
	Chemical	-	38 %	Wool	-	[121]
		-	16.6 %	Cotton		
		-	16.6 %	Flax		
	Chemical	-	< 1%	Cotton	-	[122]
	Chemical	-	35 %	Viscose	-	[123]
	Chemical	9 MPa	13.3 %	MWCNTs	-	[11]
	Chemical	65 MPa	15 %	MWCNTs	PEO-SO_3	[130]
	Thermal	7.5 MPa	49 % 16 %	Nylon 6,6 PET	-	[111]
	Thermal	-	12.1 %	PET	Ag	[10]
	Thermal	0.55 MPa	68 %	PEVA	PTFE / Al	[120]
	Thermal	-	80 %	GO	Nylon 6,6	[119]
	Thermal	55 MPa	13 %	MWCNTs	PU	[130]
	Thermal	-	87%	Polyethylene	-	[116]
	Thermal	-	-	Spandex	-	[118]
	Thermal	2.5 MPa	5.1 %	Nylon 6,6	-	[164]
	Thermal	22.6 MPa	5 %	Zirconia	-	[117]

20°C to 200°C, the muscles showed up to 80% of linear contraction or a 75% elongation, depending on the chirality. The actuation was reversible, and the devices resulted capable to lift over 100 times their own weight.

More recently, in [116], the authors used ultrahigh molecular weight polyethylene (UHMWPE) xerogel fibers, manufactured by extrusion. The coiled artificial muscle thus developed could be thermally activated by exploiting the shape memory effect, reaching maximum contractions of 87%.

To further implement biomimicry, in [118] a system of actuators consisting of two twisted and coiled bundles of Spandex (a commercial fiber based on polyurethane) capable of reproducing the functioning of an antagonistic pair of muscles such as the bicep and the triceps, was developed. To demonstrate their functionality, the authors also designed a robotic arm driven by these actuators and a validation system.

The twisting, coiling, and plying techniques were also used with many other materials to produce linear actuators. For example, natural fibers such as wool, cotton, and flax had been investigated to design miniature linear actuators [121]. These materials are highly anisotropic in response to moisture contact. These fibers were firstly twisted in yarns, then over-twisted into coiled structures. The devices were finally treated with surfactants to improve their wettability. These cotton-made actuators produced a maximum contraction of 16.6% (applied load = 20 g) and a maximum work capacity of 200 J/kg, using an applied load of 200 g (linear contraction = 7%). The wool-made actuators achieved a maximum contraction of 38% (applied load = 12 g) and a maximum work capacity of 190 J/kg, using an applied load of about 60 g (linear contraction = 15%). Finally, the flax muscles reached a maximum contraction of 16.6% (applied load = 15 g) and a maximum work capacity of 45 J/kg employing an applied load of 60 g (linear contraction = 17%).

Cotton was also used for a moisture-sensitive artificial muscle in [122]. Despite a reported torsional stroke of 42.55 °/mm and a rotational speed of 720 rpm, this actuator showed only a slight linear contraction < 1%.

Trying to produce a cheap actuator, in [123] the authors proposed a device made with fibers originating from natural sources, the viscose. This water responsive coil-shaped artificial muscle could generate a contraction of 35 %.

In [162], the focus was on the improvement and simplification of a nylon TCP muscle activation system. Trying to avoid the complex control for the heating and cooling of a TCP muscle, the authors proposed a shape memory alloy to mutate the activation mechanism into electrical. Several different specimens were produced, both twisting nylon line on a SMA wire or twisting and coiling them together. These muscles showed a contractive strain up to 44.1 %, driving up to 3.43 N of loads and providing 6.77 W/m of power density. In a later work [163], an array muscle for a soft finger with a variable stiffness was also produced.

The electrospinning technique was also applied to produce coiled and/or plied artificial muscles. A new multi-responsive coiled yarn of Nylon 6,6, driven by solvents and heating, was designed by [164]**.** The structure was manually produced over twisting a non-woven, randomly aligned, electrospun mat up to the formation of the coiled structure. Through solvent activation, the authors obtained a rotational actuator, suggesting capillary force narrowing as the activation mechanism. Through heating, instead, the actuator showed a shortening (up to 5.1% under a load that was 1380 times its weight) caused by the thermal expansion of Nylon 6,6. The reported work capacity was up to 34.5 J/Kg while the maximum stress achieved was 2.5 MPa under a 1880 loading ratio.

Later, in [117], an electrospun artificial muscle suitable for operating at high temperatures was proposed by using coiled yarns of shape-memory ceramic nanofibers (SMC). Mats of zirconia-based nanofibers were wrapped around a glass rod, resulting in SMC spring. Thanks to their shape memory, the authors obtained contractions up to 5%, with reduced recovery time (0.16 s) through thermal activation. The maximum stress obtained was 14.5-22.6 MPa, with a work density of about 15-20 KJ /m^3. These structures have also proved to be very resistant to breakage, reaching values between 100 and 200 MPa.

Some of the actuators presented in this section have also found early applications as prototypes of artificial muscles. Given their low cost and ease of production, TCP muscles are the most widespread, with examples of use in robotic hand grasping [16,165–167] or artificial muscle systems designed to imitate the principles of recruitment and variable stiffness [168,172]. For this type of muscles some mathematical models [169] have also been proposed in order to obtain valid tools for the design and control of these actuators (Table 4).

6. Conclusions and future perspectives

The topic of the fibrous soft-actuators production is extremely challenging in the smart materials research field. Skeletal muscle is a valid example of how the evolution led to a perfectly balanced actuator by exploiting at best both a hierarchical fibrous structure and the assembly and scaling up of nanometric linear actuators, the sarcomeres. Giving a comprehensive overview on the state-of-the-art for these fibrous actuators, this review underlined that, to date, the principal focus of researchers was to magnify their contractile properties. To reach this goal, various solutions were investigated, mainly through polymeric materials and CNTs. Several actuation mechanisms such as chemical, electrochemical, photochemical, thermal or electrothermal were employed. Combining these mechanisms with the classical textile manufacturing techniques (i.e. bundling, yarning, braiding, knitting or waving) or producing spring-like assemblies (i.e. coiled or plied), researchers have demonstrated the possibility to enhance the actuators linear contraction, with extremely promising outcomes. However, despite these encouraging results, no works still have proposed a proper biomimetic fabrication strategy, able to achieve a linear contraction, while closely biomimicking also the hierarchical fibrous structure of the natural muscles. Clearly, this would be a paradigm shift for the soft robotic research field, to achieve all the features that made skeletal muscles so successful: their perfectly balanced mechanical properties, their softness and most of all their linear actuation. This last attribute confers them extreme scalability and modularity, fine tuning on the control of the contraction and the stiffness, the possibility to detach the force application point and a reduced clutter. These properties, from our point of view, can presumably be reached only through the faithful reproduction of skeletal muscles hierarchical morphology from the nano- up to the macro-scale.

Declaration of Competing Interest

The authors declare no conflict of interest.

CRediT authorship contribution statement

Carlo Gotti: Conceptualization, Writing - original draft, Visualization, Investigation. **Alberto Sensini:** Conceptualization, Writing - original draft, Visualization, Investigation. **Andrea Zucchelli:** Conceptualization, Writing - review & editing, Supervision, Project administration, Funding acquisition. **Raffaella Carloni:** Conceptualization, Writing - review & editing, Supervision, Project administration, Funding acquisition. **Maria Letizia Focarete:** Conceptualization, Writing - review & editing, Supervision, Project administration, Funding acquisition.

Acknowledgements

Funding: This work was supported by the European Union within the Horizon 2020 research and innovation programme [grant number 801378 MAGNIFY project https://www.magnifyproject.eu/].

References

[1] D.T. Roper, S. Sharma, R. Sutton, P. Culverhouse, A review of developments towards biologically inspired propulsion systems for autonomous underwater vehicles, Proc. Inst. Mech. Eng. Part M 225 (2011) 77–96, doi:10.1177/1475090210397438.
[2] S. Kim, C. Laschi, B. Trimmer, Soft robotics: a bioinspired evolution in robotics, Trends Biotechnol 31 (2013) 287–294, doi:10.1016/j.tibtech.2013.03.002.
[3] C. Laschi, B. Mazzolai, M. Cianchetti, Soft robotics: technologies and systems pushing the boundaries of robot abilities, Sci. Robot. 1 (2016) eaah3690, doi:10.1126/scirobotics.aah3690.
[4] M.A. Gonzalez, W.W. Walter, An investigation of electrochemomechanical actuation of conductive Polyacrylonitrile (PAN) nanofiber composites, in: Electroact. Polym. Actuators Devices 2014, 9056, 2014, pp. 1–9, doi:10.1117/12.2049670.
[5] A.A. Zadpoor, Meta-biomaterials, Biomater. Sci. 8 (2020) 18–38, doi:10.1039/C9BM01247H.
[6] B. Salahuddin, H. Warren, G.M. Spinks, Thermally actuated hydrogel bead based braided artificial muscle, Smart Mater. Struct. 29 (2020) 055042, doi:10.1088/1361-665X/ab79ba.
[7] D. Kongahage, J. Foroughi, Actuator materials: review on recent advances and future outlook for smart textiles, Fibers 7 (2019) 21, doi:10.3390/fib7030021.
[8] W. Xu, D.H. Gracias, Soft three-dimensional robots with hard two-dimensional materials, ACS Nano 13 (2019) 4883–4892, doi:10.1021/acsnano.9b03051.
[9] S.M. Mirvakili, A. Pazukha, W. Sikkema, C.W. Sinclair, G.M. Spinks, R.H. Baughman, J.D.W. Madden, Niobium nanowire yarns and their application as artificial muscles, Adv. Funct. Mater. 23 (2013) 4311–4316, doi:10.1002/adfm.201203808.
[10] J. Park, J.W. Yoo, H.W. Seo, Y. Lee, J. Suhr, H. Moon, J.C. Koo, H.R. Choi, R. Hunt, K.J. Kim, S.H. Kim, J.-D. Nam, Electrically controllable twisted-coiled artificial muscle actuators using surface-modified polyester fibers, Smart Mater. Struct. 26 (2017) 035048, doi:10.1088/1361-665X/aa5323.
[11] K. Jin, S. Zhang, S. Zhou, J. Qiao, Y. Song, J. Di, D. Zhang, Q. Li, Self-plied and twist-stable carbon nanotube yarn artificial muscles driven by organic solvent adsorption, Nanoscale 10 (2018) 8180–8186, doi:10.1039/C8NR01300D.
[12] J.A. Lee, N. Li, C.S. Haines, K.J. Kim, X. Lepró, R. Ovalle-Robles, S.J. Kim, R.H. Baughman, Electrochemically powered, energy-conserving carbon nanotube artificial muscles, Adv. Mater. 29 (2017) 1700870, doi:10.1002/adma.201700870.
[13] J.A. Lee, Y.T. Kim, G.M. Spinks, D. Suh, X. Lepró, M.D. Lima, R.H. Baughman, S.J. Kim, All-solid-state carbon nanotube torsional and tensile artificial muscles, Nano Lett. 14 (2014) 2664–2669, doi:10.1021/nl500526r.
[14] M.D. Lima, N. Li, M. Jung de Andrade, S. Fang, J. Oh, G.M. Spinks, M.E. Kozlov, C.S. Haines, D. Suh, J. Foroughi, S.J. Kim, Y. Chen, T. Ware, M.K. Shin, L.D. Machado, A.F. Fonseca, J.D.W. Madden, W.E. Voit, D.S. Galvao, R.H. Baughman, Electrically, chemically, and photonically powered torsional and tensile actuation of hybrid carbon nanotube yarn muscles, Science 338 (2012) 928–932, doi:10.1126/science.1226762.
[15] J. Lee, S. Ko, C.H. Kwon, M.D. Lima, R.H. Baughman, S.J. Kim, Carbon nanotube yarn-based glucose sensing artificial muscle, Small. 12 (2016) 2085–2091, doi:10.1002/smll.201503509.
[16] L. Wu, M. Jung de Andrade, L.K. Saharan, R.S. Rome, R.H. Baughman, Y. Tadesse, Compact and low-cost humanoid hand powered by nylon artificial muscles, Bioinspir. Biomim. 12 (2017) 026004, doi:10.1088/1748-3190/aa52f8.
[17] L. Sutton, H. Moein, A. Rafiee, J.D.W. Madden, C. Menon, Design of an assistive wrist orthosis using conductive nylon actuators, in: Proc. IEEE RAS EMBS Int. Conf. Biomed. Robot. Biomechatronics. 2016-July, 2016, pp. 1074–1079, doi:10.1109/BIOROB.2016.7523774.
[18] W.R. Frontera, J. Ochala, Skeletal Muscle, A brief review of structure and function, Calcif. Tissue Int. 96 (2015) 183–195, doi:10.1007/s00223-014-9915-y.
[19] N. Light, A.E. Champion, Characterization of muscle epimysium, perimysium and endomysium collagens, Biochem. J. 219 (1984) 1017–1026, doi:10.1042/bj2191017.
[20] L. Shanshan, D.M. Dudek, Y. Cao, M.M. Balamurali, J. Gosline, H. Li, Designed biomaterials to mimic the mechanical properties of muscles, Nature 465 (2010) 69–73, doi:10.1038/nature09024.
[21] A.R. Gillies, R.L. Lieber, Structure and function of the skeletal muscle extracellular matrix, Muscle Nerve 44 (2011) 318–331, doi:10.1002/mus.22094.
[22] M. Shahinpoor, K.J. Kim, M. Mojarrad, Anatomy and physiology of human muscle, in: Artif. Muscles - Appl. Adv. Polym. Nanocomposites, first ed., Taylor & Francis, 2007, p. 482.
[23] T. Toursel, L. Stevens, H. Granzier, Y. Mounier, Passive tension of rat skeletal soleus muscle fibers: effects of unloading conditions, J. Appl. Physiol. 92 (2002) 1465–1472, doi:10.1152/japplphysiol.00621.2001.
[24] Y.C. Fung, Biomechanics: Mechanical Properties of Living Tissues, second ed., Springer US, New York, 1993, doi:10.1007/978-1-4757-2257-4.
[25] K.W. VanDusen, L.M. Larkin, Muscle-tendon interface, in: J.W. F., C.T.L. Syam, P. Nukavarapu (Eds.), Regen. Eng. Musculoskelet. Tissues Interfaces, Woodhead P, Elsevier, Cambridge, 2015, pp. 409–429, doi:10.1016/B978-1-78242-301-0.00017-3.
[26] R. Herbert, The passive mechanical properties of muscle and their adaptations to altered patterns of use, Aust. J. Physiother. 34 (1988) 141–149, doi:10.1016/S0004-9514(14)60606-1.
[27] G.C. Sieck, L.F. Ferreira, M.B. Reid, C.B. Mantilla, Mechanical properties of respiratory muscles, in: Compr. Physiol., John Wiley & Sons, Inc., Hoboken, NJ, USA, 2013, pp. 1533–1567, doi:10.1002/cphy.c130003.
[28] A. Magid, D. Law, Myofibrils bear most of the resting tension in frog skeletal muscle, Science 230 (1985) 1280–1282, doi:10.1126/science.4071053.
[29] U. Proske, D.L. Morgan, Do cross-bridges contribute to the tension during stretch of passive muscle? J. Muscle Res. Cell Motil. 20 (1999) 433–442, doi:10.1023/a:1005573625675.
[30] J.-P. Rospars, N. Meyer-Vernet, Force per cross-sectional area from molecules to muscles: a general property of biological motors, R. Soc. Open Sci. 3 (2016) 160313, doi:10.1098/rsos.160313.
[31] L.E. Bilston, K. Tan, Measurement of passive skeletal muscle mechanical properties in vivo: recent progress, clinical applications, and remaining challenges, Ann. Biomed. Eng. 43 (2014) 261–273, doi:10.1007/s10439-014-1186-2.
[32] T.J. Roberts, Contribution of elastic tissues to the mechanics and energetics of muscle function during movement, J. Exp. Biol. 219 (2016) 266–275, doi:10.1242/jeb.124446.
[33] J.L. Gennisson, T. Deffieux, E. Macé, G. Montaldo, M. Fink, M. Tanter, Viscoelastic and anisotropic mechanical properties of in vivo muscle tissue assessed by supersonic shear imaging, Ultrasound Med. Biol. 36 (2010) 789–801, doi:10.1016/j.ultrasmedbio.2010.02.013.
[34] Y. Yoshikawa, T. Yasuike, A. Yagi, T. Yamada, Transverse elasticity of myofibrils of rabbit skeletal muscle studied by atomic force microscopy, Biochem. Biophys. Res. Commun. 256 (1999) 13–19, doi:10.1006/bbrc.1999.0279.
[35] A.B. Mathur, G.A. Truskey, W.M. Reichert, Atomic force and total internal reflection fluorescence microscopy for the study of force transmission in endothelial cells, Biophys. J. 78 (2000) 1725–1735, doi:10.1016/S0006-3495(00)76724-5.
[36] P.D. Hoang, R.D. Herbert, G. Todd, R.B. Gorman, S.C. Gandevia, Passive mechanical properties of human gastrocnemius muscle-tendon units, muscle fascicles and tendons in vivo, J. Exp. Biol. 210 (2007) 4159–4168, doi:10.1242/jeb.002204.
[37] S. Schleifenbaum, M. Schmidt, R. Möbius, T. Wolfskämpf, C. Schröder, R. Grunert, N. Hammer, T. Prietzel, Load and failure behavior of human muscle samples in the context of proximal femur replacement, BMC Musculoskelet. Disord. 17 (2016) 149, doi:10.1186/s12891-016-0998-7.
[38] V. Kovanen, H. Suominen, E. Heikkinen, Mechanical properties of fast and slow skeletal muscle with special reference to collagen and endurance training, J. Biomech. 17 (1984) 725–735, doi:10.1016/0021-9290(84)90103-9.
[39] I.V. Ogneva, D.V. Lebedev, B.S. Shenkman, Transversal stiffness and young's modulus of single fibers from rat soleus muscle probed by atomic force microscopy, Biophys. J. 98 (2010) 418–424, doi:10.1016/j.bpj.2009.10.028.
[40] S. Bensamoun, L. Stevens, M.J. Fleury, G. Bellon, F. Goubel, M.C. Ho Ba Tho, Macroscopic–microscopic characterization of the passive mechanical properties in rat soleus muscle, J. Biomech. 39 (2006) 568–578, doi:10.1016/j.jbiomech.2004.04.036.
[41] E. Defranchi, E. Bonaccurso, M. Tedesco, M. Canato, E. Pavan, R. Raiteri, C. Reggiani, Imaging and elasticity measurements of the sarcolemma of fully differentiated skeletal muscle fibres, Microsc. Res. Tech. 67 (2005) 27–35, doi:10.1002/jemt.20177.
[42] C.D. Kuthe, R.V. Uddanwadiker, Investigation of effect of fiber orientation on mechanical behavior of skeletal muscle, J. Appl. Biomater. Funct. Mater. 14 (2016) e154–e162, doi:10.5301/jabfm.5000275.
[43] M. Lakie, L.G. Robson, Thixotropy: the effect of stretch size in relaxed frog muscle, Q. J. Exp. Physiol. 73 (1988) 127–129, doi:10.1113/expphysiol.1988.sp003110.
[44] A.V. Wolff, A.K. Niday, K.A. Voelker, J.A. Call, N.P. Evans, K.P. Granata, R.W. Grange, Passive mechanical properties of maturing extensor digitorum longus are not affected by lack of dystrophin, Muscle Nerve 34 (2006) 304–312, doi:10.1002/mus.20588.
[45] R.L. Moss, W. Halpern, Elastic and viscous properties of resting frog skeletal muscle, Biophys. J. 17 (1977) 213–228, doi:10.1016/S0006-3495(77)85651-8.
[46] R.L. Lieber, M.E. Leonard, C.G. Brown, C.L. Trestik, Frog semitendinosis tendon load-strain and stress-strain properties during passive loading, Am. J. Physiol. 261 (1991) C86–C92, doi:10.1016/S1381-1169(99)00316-7.
[47] C.N. Maganaris, V. Baltzopoulos, D. Ball, A.J. Sargeant, In vivo specific tension of human skeletal muscle, J. Appl. Physiol. 90 (2001) 865–872, doi:10.1152/jappl.2001.90.3.865.
[48] T.A. Mcmahon, Muscles, Reflexes, and Locomotion, Priceton University Press, Priceton, New jersey, 1984.
[49] D.E. Rassier, Muscle Biophysics, Springer New York, New York, NY, 2010, doi:10.1007/978-1-4419-6366-6.
[50] N.G. Koulouris, I. Dimitroulis, Structure and function of the respiratory muscles, Pneumon 14 (2001) 91–108.
[51] T.F. Otero, Artificial muscles driven by the cooperative actuation of electrochemical molecular machines. Persistent discrepancies and challenges, Int. J. Smart Nano Mater. 8 (2017) 125–143, doi:10.1080/19475411.2018.1434256.
[52] N.-K. Persson, J.G. Martinez, Y. Zhong, A. Maziz, E.W.H. Jager, Actuating textiles: next generation of smart textiles, Adv. Mater. Technol. 3 (2018) 1700397, doi:10.1002/admt.201700397.

[53] J.D. Madden, Mobile robots: motor challenges and materials solutions, Science 318 (2007) 1094–1097, doi:10.1126/science.1146351.
[54] J.M. Hollerback, I.W. Hunter, J. Ballantyne, A comparative analysis of actuator technologies for robotics, in: Robot. Rev. 2, MIT Press, Cambridge, MA; USA, 1992, pp. 299–342.
[55] K. Asaka, H. Okuzaki, Soft Actuators, Springer, Japan, Tokyo, 2014, doi:10.1007/978-4-431-54767-9.
[56] C. Lee, M. Kim, Y.J. Kim, N. Hong, S. Ryu, H.J. Kim, S. Kim, Soft robot review, Int. J. Control. Autom. Syst. 15 (2017) 3–15, doi:10.1007/s12555-016-0462-3.
[57] D. Rus, M.T. Tolley, Design, fabrication and control of soft robots, Nature 521 (2015) 467–475, doi:10.1038/nature14543.
[58] A. Maziz, A. Concas, A. Khaldi, J. Stålhand, N.K. Persson, E.W.H. Jager, Knitting and weaving artificial muscles, Sci. Adv. 3 (2017) e1600327, doi:10.1126/sciadv.1600327.
[59] E. Smela, Conjugated polymer actuators for biomedical applications, Adv. Mater. 15 (2003) 481–494, doi:10.1002/adma.200390113.
[60] J. Deng, Y. Xu, S. He, P. Chen, L. Bao, Y. Hu, B. Wang, X. Sun, H. Peng, Preparation of biomimetic hierarchically helical fiber actuators from carbon nanotubes, Nat. Protoc. 12 (2017) 1349–1358, doi:10.1038/nprot.2017.038.
[61] B. Kang Gu, Y.A. Ismail, G.M. Spinks, S.I. Kim, I. So, S.J. Kim, A linear actuation of polymeric nanofibrous bundle for artificial muscles, Chem. Mater. 21 (2009) 2689–2690, doi:10.1021/cm903343t.
[62] J. Foroughi, G.M. Spinks, S. Aziz, A. Mirabedini, A. Jeiranikhameneh, G.G. Wallace, M.E. Kozlov, R.H. Baughman, Knitted carbon-nanotube-sheath/spandex-core elastomeric yarns for artificial muscles and strain sensing, ACS Nano 10 (2016) 9129–9135, doi:10.1021/acsnano.6b04125.
[63] G.V. Stoychev, L. Ionov, Actuating fibers: design and applications, ACS Appl. Mater. Interfaces. 8 (2016) 24281–24294, doi:10.1021/acsami.6b07374.
[64] J. Li, W. Ma, L. Song, Z. Niu, L. Cai, Q. Zeng, X. Zhang, H. Dong, D. Zhao, W. Zhou, S. Xie, Superfast-response and ultrahigh-power-density electromechanical actuators based on hierarchal carbon nanotube electrodes and chitosan, Nano Lett. 11 (2011) 4636–4641, doi:10.1021/nl202132m.
[65] J.G. Martinez, K. Richter, N.-K. Persson, E.W.H. Jager, Investigation of electrically conducting yarns for use in textile actuators, Smart Mater. Struct. 27 (2018) 074004, doi:10.1088/1361-665X/aabab5.
[66] C. Lee, M. Kim, Y.J. Kim, N. Hong, S. Ryu, H.J. Kim, S. Kim, Soft robot review, Int. J. Control. Autom. Syst. 15 (2017) 3–15, doi:10.1007/s12555-016-0462-3.
[67] Y. Imura, R.M.C. Hogan, M. Jaffe, Dry spinning of synthetic polymer fibers, in: Adv. Filam. Yarn Spinn. Text. Polym., Elsevier, 2014, pp. 187–202, doi:10.1533/9780857099174.2.187.
[68] R. Chokshi, H. Zia, Hot-melt extrusion technique: a review, Iran. J. Pharm. Res. 3 (2014) 3–16, doi:10.1016/S0939-6411(02)00061-9.
[69] Y. Lu, S.C. Chen, Micro and nano-fabrication of biodegradable polymers for drug delivery, Adv. Drug Deliv. Rev. 56 (2004) 1621–1633, doi:10.1016/j.addr.2004.05.002.
[70] S.-H. Lee, S.-M. Park, Y. Kim, Effect of the concentration of sodium acetate (SA) on crosslinking of chitosan fiber by epichlorohydrin (ECH) in a wet spinning system, Carbohydr. Polym. 70 (2007) 53–60, doi:10.1016/j.carbpol.2007.03.002.
[71] R.A. O'Connor, G.B. McGuinness, Electrospun nanofibre bundles and yarns for tissue engineering applications: a review, Proc. Inst. Mech. Eng. Part H 230 (2016) 987–998, doi:10.1177/0954411916656664.
[72] A. Sensini, L. Cristofolini, Biofabrication of electrospun scaffolds for the regeneration of tendons and ligaments, Materials (Basel) 11 (2018) 1963, doi:10.3390/ma11101963.
[73] W. Liu, S. Thomopoulos, Y. Xia, Electrospun nanofibers for regenerative medicine, Adv. Healthc. Mater. 1 (2012) 10–25, doi:10.1002/adhm.201100021.
[74] X. Li, J. Xie, J. Lipner, X. Yuan, S. Thomopoulos, Y. Xia, Nanofiber scaffolds with gradations in mineral content for mimicking the tendon-to-bone insertion site, Nano Lett. 9 (2009) 2763–2768, doi:10.1021/nl901582f.
[75] S. Sahoo, H. Ouyang, J.C.-H. Goh, T.E. Tay, S.L. Toh, Characterization of a novel polymeric scaffold for potential application in tendon/ligament tissue engineering, Tissue Eng 12 (2006) 91–99, doi:10.1089/ten.2006.12.91.
[76] G. Verdiyeva, K. Koshy, N. Glibbery, H. Mann, A.M. Seifalian, Tendon reconstruction with tissue engineering approach - a review, J. Biomed. Nanotechnol. 11 (2015) 1495–1523, doi:10.1166/jbn.2015.2121.
[77] A. Sensini, C. Gualandi, L. Cristofolini, G. Tozzi, M. Dicarlo, G. Teti, M. Mattiolibelmonte, M.L. Focarete, Biofabrication of bundles of poly (lactic acid)-collagen blends mimicking the fascicles of the human Achille tendon, Biofabrication 9 (2017) 015025, doi:10.1088/1758-5090/aa6204.
[78] L. Jia, M.P. Prabhakaran, X. Qin, S. Ramakrishna, Guiding the orientation of smooth muscle cells on random and aligned polyurethane/collagen nanofibers, J. Biomater. Appl. 29 (2014) 364–377, doi:10.1177/0885328214529002.
[79] H. Liu, X. Ding, G. Zhou, P. Li, X. Wei, Y. Fan, Electrospinning of nanofibers for tissue engineering applications, J. Nanomater. 2013 (2013) 495708, doi:10.1155/2013/495708.
[80] A. Haider, S. Haider, I.K. Kang, A comprehensive review summarizing the effect of electrospinning parameters and potential applications of nanofibers in biomedical and biotechnology, Arab. J. Chem. 11 (2015) 1165–1188, doi:10.1016/j.arabjc.2015.11.015.
[81] H.-S. Bae, A. Haider, K.M.K. Selim, D.-Y. Kang, E.-J. Kim, I.-K. Kang, Fabrication of highly porous PMMA electrospun fibers and their application in the removal of phenol and iodine, J. Polym. Res. 20 (2013) 158, doi:10.1007/s10965-013-0158-9.
[82] S.A. Sell, M.J. McClure, K. Garg, P.S. Wolfe, G.L. Bowlin, Electrospinning of collagen/biopolymers for regenerative medicine and cardiovascular tissue engineering, Adv. Drug Deliv. Rev. 61 (2009) 1007–1019, doi:10.1016/j.addr.2009.07.012.
[83] U. Ali, Y. Zhou, X. Wang, T. Lin, Electrospinning of continuous nanofiber bundles and twisted nanofiber yarns, nanofiber-production, Prop. Funct. Appl. (2011) 153–174, doi:10.5772/25059.
[84] N.H.A. Ngadiman, M. Noordin, A. Idris, D. Kurniawan, A review of evolution of electrospun tissue engineering scaffold: from two dimensions to three dimensions, Proc. Inst. Mech. Eng. Part H 231 (2017) 597–616, doi:10.1177/0954411917699021.
[85] T. Jiang, E.J. Carbone, K.W.H. Lo, C.T. Laurencin, Electrospinning of polymer nanofibers for tissue regeneration, Prog. Polym. Sci. 46 (2015) 46, doi:10.1016/j.progpolymsci.2014.12.001.
[86] K.D. McKeon-Fischer, D.H. Flagg, J.W. Freeman, Poly(acrylic acid)/poly(vinyl alcohol) compositions coaxially electrospun with poly(ε-caprolactone) and multi-walled carbon nanotubes to create nanoactuating scaffolds, Polymer 52 (2011) 4736–4743, doi:10.1016/j.polymer.2011.08.012.
[87] K.D. McKeon-Fischer, D.H. Flagg, J.W. Freeman, Coaxial electrospun poly(ε-caprolactone), multiwalled carbon nanotubes, and polyacrylic acid/polyvinyl alcohol scaffold for skeletal muscle tissue engineering, J. Biomed. Mater. Res. 99 A (2011) 493–499, doi:10.1002/jbm.a.33116.
[88] K.D. McKeon-Fischer, D.P. Browe, R.M. Olabisi, J.W. Freeman, Poly(3,4-ethylenedioxythiophene) nanoparticle and poly(ε-caprolactone) electrospun scaffold characterization for skeletal muscle regeneration, J. Biomed. Mater. Res. 103 (2015) 3633–3641, doi:10.1002/jbm.a.35481.
[89] D. Sun, C. Chang, S. Li, L. Lin, Near-field electrospinning, Nano Lett. 6 (2006) 839–842, doi:10.1021/nl0602701.
[90] G.S. Bisht, G. Canton, A. Mirsepassi, L. Kulinsky, S. Oh, D. Dunn-Rankin, M.J. Madou, Controlled continuous patterning of polymeric nanofibers on three-dimensional substrates using low-voltage near-field electrospinning, Nano Lett 11 (2011) 1831–1837, doi:10.1021/nl2006164.
[91] C. Chang, K. Limkrailassiri, L. Lin, Continuous near-field electrospinning for large area deposition of orderly nanofiber patterns, Appl. Phys. Lett. 93 (2008) 1–4, doi:10.1063/1.2975834.
[92] G. Zheng, W. Li, X. Wang, D. Wu, D. Sun, L. Lin, Precision deposition of a nanofibre by near-field electrospinning, J. Phys. D. 43 (2010) 1–6, doi:10.1088/0022-3727/43/41/415501.
[93] M. Kumar, Y. Ando, Chemical vapor deposition of carbon nanotubes: a review on growth mechanism and mass production, J. Nanosci. Nanotechnol. 10 (2010) 3739–3758, doi:10.1166/jnn.2010.2939.
[94] K. Choy, Chemical vapour deposition of coatings, Prog. Mater. Sci. 48 (2003) 57–170, doi:10.1016/S0079-6425(01)00009-3.
[95] Á. Kukovecz, G. Kozma, Z. Kónya, Multi-walled carbon nanotubes, in: R. Vajtai (Ed.), Springer Handb. Nanomater., Springer, 2013, pp. 1–1221, doi:10.1007/978-3-642-20595-8.
[96] Y. Song, S. Zhou, K. Jin, J. Qiao, D. Li, C. Xu, D. Hu, J. Di, M. Li, Z. Zhang, Q. Li, Hierarchical carbon nanotube composite yarn muscles, Nanoscale 10 (2018) 4077–4084, doi:10.1039/c7nr08595h.
[97] J. Foroughi, G. Spinks, Carbon nanotube and graphene fiber artificial muscles, Nanoscale Adv. 1 (2019) 4592–4614, doi:10.1039/c9na00038k.
[98] T. Mirfakhrai, J.D.W. Madden, R.H. Baughman, Polymer artificial muscles, Mater. Today. 10 (2007) 30–38, doi:10.1016/S1369-7021(07)70048-2.
[99] S. Lin, Z. Wang, X. Chen, J. Ren, S. Ling, Ultrastrong and highly sensitive fiber microactuators constructed by force-reeled silks, Adv. Sci. (2020) 1902743, doi:10.1002/advs.201902743.
[100] S.Y. Severt, S.L. Maxwell, J.S. Bontrager, J.M. Leger, A.R. Murphy, Mimicking muscle fiber structure and function through electromechanical actuation of electrospun silk fiber bundles, J. Mater. Chem. B. 5 (2017) 8105–8114, doi:10.1039/C7TB01904A.
[101] V. Balzani, A. Credi, M. Venturi, Molecular Devices and Machines, Wiley, 2008, doi:10.1002/9783527621682.
[102] C.J. Bruns, J.F. Stoddart, Rotaxane-based molecular muscles, Acc. Chem. Res. 47 (2014) 2186–2199, doi:10.1021/ar500138u.
[103] A. Coskun, M. Banaszak, R.D. Astumian, J.F. Stoddart, B.A. Grzybowski, Great expectations: can artificial molecular machines deliver on their promise? Chem. Soc. Rev. 41 (2012) 19–30, doi:10.1039/c1cs15262a.
[104] F. Lancia, A. Ryabchun, A.D. Nguindjel, S. Kwangmettatam, N. Katsonis, Mechanical adaptability of artificial muscles from nanoscale molecular action, Nat. Commun. 10 (2019) 1–8, doi:10.1038/s41467-019-12786-2.
[105] J. Chen, F.K.C. Leung, M.C.A. Stuart, T. Kajitani, T. Fukushima, E. Van Der Giessen, B.L. Feringa, Artificial muscle-like function from hierarchical supramolecular assembly of photoresponsive molecular motors, Nat. Chem. 10 (2018) 132–138, doi:10.1038/nchem.2887.
[106] C.-H. Hong, S.-J. Ki, J.-H. Jeon, H. Che, I.-K. Park, C.-D. Kee, I.-K. Oh, Electroactive bio-composite actuators based on cellulose acetate nanofibers with specially chopped polyaniline nanoparticles through electrospinning, Compos. Sci. Technol. 87 (2013) 135–141, doi:10.1016/j.compscitech.2013.08.006.
[107] R. Samatham, K. Choe, K.J. Kimi, M. Shahinpoor, J. Nam, Towards nano-biomimetic muscles : polyacrylonitrile nanofibers, in: Smart Struct. Mater. 2004 Electroact. Polym. Actuators Devices, 5385, 2004, pp. 235–241, doi:10.1117/12.534363.
[108] I.D. Norris, M. Shahinpoor, B.R. Mattes, K.J. Kim, L.O. Sillerud, Electroactive polyacrylonitrile nanofibers as artificial nano-muscles, in: Smart Struct. Mater. 2002 Electroact. Polym. Actuators Devices, 4695, 2002, pp. 351–358, doi:10.1117/12.475181.

[109] P. Chen, Y. Xu, S. He, X. Sun, S. Pan, J. Deng, D. Chen, H. Peng, Hierarchically arranged helical fibre actuators driven by solvents and vapours, Nat. Nanotechnol. 10 (2015) 1077–1083, doi:10.1038/nnano.2015.198.
[110] F. Hu, Y. Xue, J. Xu, B. Lu, PEDOT-based conducting polymer actuators, Front. Robot. AI 6 (2019) 114, doi:10.3389/frobt.2019.00114.
[111] C.S. Haines, M.D. Lima, N. Li, G.M. Spinks, J. Foroughi, J.D.W. Madden, S.H. Kim, S. Fang, M. Jung de Andrade, F. Goktepe, O. Goktepe, S.M. Mirvakili, S. Naficy, X. Lepro, J. Oh, M.E. Kozlov, S.J. Kim, X. Xu, B.J. Swedlove, G.G. Wallace, R.H. Baughman, Artificial muscles from fishing line and sewing thread, Science 343 (2014) 868–872, doi:10.1126/science.1246906.
[112] S.-S. Kim, C.-D. Kee, Electro-active polymer actuator based on PVDF with bacterial cellulose nano-whiskers (BCNW) via electrospinning method, Int. J. Precis. Eng. Manuf. 15 (2014) 315–321, doi:10.1007/s12541-014-0340-y.
[113] A. Gestos, P.G. Whitten, G.G. Wallace, G.M. Spinks, Actuating individual electrospun hydrogel nanofibres, Soft Matter 8 (2012) 8082–8087, doi:10.1039/c2sm25387a.
[114] J. Li, S. Vadahanambi, C.D. Kee, I.K. Oh, Electrospun fullerenol-cellulose biocompatible actuators, Biomacromolecules 12 (2011) 2048–2054, doi:10.1021/bm2004252.
[115] S.M. Mirvakili, A. Rafie Ravandi, I.W. Hunter, C.S. Haines, N. Li, J. Foroughi, S. Naficy, G.M. Spinks, R.H. Baughman, J.D.W. Madden, Simple and strong: twisted silver painted nylon artificial muscle actuated by Joule heating, Electroact. Polym. Actuators Devices 2014, 9056, 2014, doi:10.1117/12.2046411.
[116] A.V. Maksimkin, I.I. Larin, D.I. Chukov, M.Y. Zadorozhnyy, T. Dayyoub, V.Y. Zadorozhnyy, F. Spieckermann, V. Soprunyuk, Coiled artificial muscles based on UHMWPE with large muscle stroke, Mater. Today Commun. 21 (2019) 100688, doi:10.1016/j.mtcomm.2019.100688.
[117] Z. Du, X. Zhou, P. Ye, X. Zeng, C.L. Gan, Shape-memory actuation in aligned zirconia nanofibers for artificial muscle applications at elevated temperatures, ACS Appl. Nano Mater. 3 (2020) 2156–2166, doi:10.1021/acsanm.9b02073.
[118] D. Cho, N. Hoepker, M.W. Frey, Fabrication and characterization of conducting polyvinyl alcohol nanofibers, Mater. Lett. 68 (2012) 293–295, doi:10.1016/j.matlet.2011.10.109.
[119] H. Kim, J.H. Moon, T.J. Mun, T.G. Park, G.M. Spinks, G.G. Wallace, S.J. Kim, Thermally responsive torsional and tensile fiber actuator based on graphene oxide, ACS Appl. Mater. Interfaces. 10 (2018) 32760–32764, doi:10.1021/acsami.8b12426.
[120] J. Fan, G. Li, High performance and tunable artificial muscle based on two-way shape memory polymer, RSC Adv. 7 (2017) 1127–1136, doi:10.1039/C6RA25024F.
[121] X. Yang, W. Wang, M. Miao, Moisture-responsive natural fiber coil-structured artificial muscles, ACS Appl. Mater. Interfaces. 10 (2018) 32256–32264, doi:10.1021/acsami.8b12144.
[122] Y. Li, X. Leng, J. Sun, X. Zhou, W. Wu, H. Chen, Z. Liu, Moisture-sensitive torsional cotton artificial muscle and textile, Chin. Phys. B. 29 (2020) 048103, doi:10.1088/1674-1056/ab7745.
[123] Y. Li, M. Miao, Water-responsive artificial muscles from commercial viscose fibers without chemical treatment, Mater. Res. Lett. 8 (2020) 232–238, doi:10.1080/21663831.2020.1743787.
[124] K. Katayama, M. Tsuji, Fundamentals of spinning, in: T. Nakajima (Ed.), Adv. Fiber Spinn. Technol., fifth ed., Woodhead Publishing Limited, Oxford, 1994, p. 256, doi:10.1533/9781845693213.
[125] J. Foroughi, G.M. Spinks, D. Antiohos, A. Mirabedini, S. Gambhir, G.G. Wallace, S.R. Ghorbani, G. Peleckis, M.E. Kozlov, M.D. Lima, R.H. Baughman, Highly conductive carbon nanotube-graphene hybrid yarn, Adv. Funct. Mater. 24 (2014) 5859–5865, doi:10.1002/adfm.201401412.
[126] H.B. Schreyer, M. Shahinpoor, K.J. Kim, Electrical activation of PAN-Pt artificial muscles, in: Electroact. Polym. Actuators Devices 1999, 3669, 1999, pp. 192–198, doi:10.1117/12.349676.
[127] K.-Y. Chun, S. Hyeong Kim, M. Kyoon Shin, C. Hoon Kwon, J. Park, Y. Tae Kim, G.M. Spinks, M.D. Lima, C.S. Haines, R.H. Baughman, S. Jeong Kim, Hybrid carbon nanotube yarn artificial muscle inspired by spider dragline silk, Nat. Commun. 5 (2014) 3322, doi:10.1038/ncomms4322.
[128] S.H. Kim, C.H. Kwon, K. Park, T.J. Mun, X. Lepró, R.H. Baughman, G.M. Spinks, S.J. Kim, Bio-inspired, moisture-powered hybrid carbon nanotube yarn muscles, Sci. Rep. 6 (2016) 23016, doi:10.1038/srep23016.
[129] J. Foroughi, G.M. Spinks, G.G. Wallace, J. Oh, M.E. Kozlov, S. Fang, T. Mirfakhrai, J.D.W. Madden, M.K. Shin, S.J. Kim, R.H. Baughman, Torsional carbon nanotube artificial muscles, Science 334 (2011) 494–497, doi:10.1126/science.1211220.
[130] J. Mu, M.J. De Andrade, S. Fang, X. Wang, E. Gao, N. Li, S.H. Kim, H. Wang, C. Hou, Q. Zhang, M. Zhu, D. Qian, H. Lu, D. Kongahage, S. Talebian, J. Foroughi, G. Spinks, H. Kim, T.H. Ware, H.J. Sim, D.Y. Lee, Y. Jang, S.J. Kim, R.H. Baughman, Sheath-run artificial muscles, Science 365 (2019) 150–155, doi:10.1126/science.aaw2403.
[131] C.R. Carlisle, C. Coulais, M. Namboothiry, D.L. Carroll, R.R. Hantgan, M. Guthold, The mechanical properties of individual, electrospun fibrinogen fibers, Biomaterials 30 (2009) 1205–1213, doi:10.1016/j.biomaterials.2008.11.006.
[132] J. Pu, X. Yan, Y. Jiang, C. Chang, L. Lin, Piezoelectric actuation of direct-write electrospun fibers, Sensors Actuators A Phys 164 (2010) 131–136, doi:10.1016/j.sna.2010.09.019.
[133] K. Salehpoor, M. Shahinpoor, M. Mojarrad, Electrically controllable artificial PAN muscles, Proc. SPIE. 2716 (1996) 116–124, doi:10.1117/12.232131.
[134] K. Salehpoor, M. Shahinpoor, M. Mojarrad, Some experimental results on the dynamic performance of PAN muscles, in: Smart Struct. Mater. 1997 Smart Mater. Technol., 3040, 1997, pp. 169–173, doi:10.1117/12.267111.
[135] H.B. Schreyer, N. Gebhart, K.J. Kim, M. Shahinpoor, Electrical activation of artificial muscles containing polyacrylonitrile gel fibers, Biomacromolecules 1 (2000) 642–647, doi:10.1021/bm005557l.
[136] R. Samatham, I.-S. Park, K.J. Kim, J.-D. Nam, N. Whisman, J. Adams, Electrospun nanoscale polyacrylonitrile artificial muscle, Smart Mater. Struct. 15 (2006) N152–N156, doi:10.1088/0964-1726/15/6/N03.
[137] M. Naraghi, I. Chasiotis, Mechanics of PAN nanofiber, in: I.M. Daniel, E.E. Gdoutos, Y.D.S. Rajapakse (Eds.), Major Accompl. Compos. Mater. Sandw. Struct., Springer, Netherlands, Dordrecht, 2010, pp. 757–777, doi:10.1007/978-90-481-3141-9.
[138] M. Naraghi, S.N. Arshad, I. Chasiotis, Molecular orientation and mechanical property size effects in electrospun polyacrylonitrile nanofibers, Polymer 52 (2011) 1612–1618, doi:10.1016/j.polymer.2011.02.013.
[139] A.S. Hutchison, T.W. Lewis, S.E. Moulton, G.M. Spinks, G.G. Wallace, Development of polypyrrole-based electromechanical actuators, Synth. Met. 113 (2000) 121–127, doi:10.1016/S0379-6779(00)00190-9.
[140] M. Shahinpoor, K.J. Kim, H.B. Schreyer, Artificial sarcomere and muscle made with conductive polyacrylonitrile (C-PAN) fiber bundles, in: Smart Struct. Mater. 2000 Electroact. Polym. Actuators Devices, 3987, 2000, p. 243, doi:10.1117/12.387783.
[141] M. Zhang, Multifunctional carbon nanotube yarns by downsizing an ancient technology, Science 306 (2004) 1358–1361, doi:10.1126/science.1104276.
[142] T. Mirfakhrai, J. Oh, M. Kozlov, E.C.W. Fok, M. Zhang, S. Fang, R.H. Baughman, J.D.W. Madden, Electrochemical actuation of carbon nanotube yarns, Smart Mater. Struct. 16 (2007) S243–S249, doi:10.1088/0964-1726/16/2/S07.
[143] I.W. Hunter, S. Lafontaine, A comparison of muscle with artificial actuators, in: Tech. Dig. IEEE Solid-State Sens. Actuator Work, 1992, pp. 178–185, doi:10.1109/SOLSEN.1992.228297.
[144] Y. Bar-cohen, Electroactive polymers as artificial muscles - reality and challenges, 19th AIAA Appl. Aerodyn. Conf., 2001, doi:10.2514/6.2001-1492.
[145] W. Guo, C. Liu, F. Zhao, X. Sun, Z. Yang, T. Chen, X. Chen, L. Qiu, X. Hu, H. Peng, A novel electromechanical actuation mechanism of a carbon nanotube fiber, Adv. Mater. 24 (2012) 5379–5384, doi:10.1002/adma.201201845.
[146] D. Liu, L. Yu, Y. He, K. Peng, J. Liu, J. Guan, D.J. Dunstan, Peculiar torsion dynamical response of spider dragline silk, Appl. Phys. Lett. 111 (2017) 013701, doi:10.1063/1.4990676.
[147] E. Wenk, H.P. Merkle, L. Meinel, Silk fibroin as a vehicle for drug delivery applications, J. Control. Release. 150 (2011) 128–141, doi:10.1016/j.jconrel.2010.11.007.
[148] Y. Wang, H.-J. Kim, G. Vunjak-Novakovic, D.L. Kaplan, Stem cell-based tissue engineering with silk biomaterials, Biomaterials 27 (2006) 6064–6082, doi:10.1016/j.biomaterials.2006.07.008.
[149] M.C. Jimenez-Molero, C. Dietrich-Buchecker, J.-P. Sauvage, Towards artificial muscles at the nanometric level, Chem. Commun. (2003) 1613–1616, doi:10.1039/b302326p.
[150] J.P. Collin, C. Dietrich-Buchecker, P. Gaviña, M.C. Jimenez-Molero, J.P. Sauvage, Shuttles and muscles: linear molecular machines based on transition metals, Acc. Chem. Res. 34 (2001) 477–487, doi:10.1021/ar0001766.
[151] M.C. Jiménez, C. Dietrich-Buchecker, J. Sauvage, Towards synthetic molecular muscles: contraction and stretching of a linear rotaxane dimer, Angew. Chem. 39 (2000) 3284–3287, doi:10.1002/1521-3773(20000915)39:183284::AID-ANIE32843.0.CO;2-7.
[152] W. Son, S. Chun, J.M. Lee, Y. Lee, J. Park, D. Suh, D.W. Lee, H. Jung, Y.-J. Kim, Y. Kim, S.M. Jeong, S.K. Lim, C. Choi, Highly twisted supercoils for superelastic multi-functional fibres, Nat. Commun. 10 (2019) 426, doi:10.1038/s41467-018-08016-w.
[153] S. Aziz, S. Naficy, J. Foroughi, H.R. Brown, G.M. Spinks, Controlled and scalable torsional actuation of twisted nylon 6 fiber, J. Polym. Sci. Part B 54 (2016) 1278–1286, doi:10.1002/polb.24035.
[154] M.D. Lima, S. Fang, X. Lepro, C. Lewis, R. Ovalle-Robles, J. Carretero-Gonzalez, E. Castillo-Martinez, M.E. Kozlov, J. Oh, N. Rawat, C.S. Haines, M.H. Haque, V. Aare, S. Stoughton, A.A. Zakhidov, R.H. Baughman, Biscrolling nanotube sheets and functional guests into yarns, Science 331 (2011) 51–55, doi:10.1126/science.1195912.
[155] Z.-L. Zhao, H.-P. Zhao, J.-S. Wang, Z. Zhang, X.-Q. Feng, Mechanical properties of carbon nanotube ropes with hierarchical helical structures, J. Mech. Phys. Solids. 71 (2014) 64–83, doi:10.1016/j.jmps.2014.06.005.
[156] X. Chen, L. Mahadevan, A. Driks, O. Sahin, Bacillus spores as building blocks for stimuli-responsive materials and nanogenerators, Nat. Nanotechnol. 9 (2014) 137–141, doi:10.1038/nnano.2013.290.
[157] D.X. Dang, T.K. Truong, S.C. Lim, D. Suh, In situ multi-dimensional actuation measurement method for tensile actuation of paraffin-infiltrated multi-wall carbon nanotube yarns, Rev. Sci. Instrum. 88 (2017) 075001, doi:10.1063/1.4990712.
[158] N.A. Atikah, L.Y. Weng, A. Anuar, C.C. Fat, I.Z. Abidin, K.S.M. Sahari, Development of nylon-based artificial muscles for the usage in robotic prosthetic limb, in: AIP Conf. Proc., 1883, 2017, doi:10.1063/1.5002060.
[159] C.S. Haines, N. Li, G.M. Spinks, A.E. Aliev, J. Di, R.H. Baughman, New twist on artificial muscles, Proc. Natl. Acad. Sci. U. S. A. 113 (2016) 11709–11716, doi:10.1073/pnas.1605273113.
[160] J.L. Lombardi, P. Calvert, Extrusion freeforming of Nylon 6 materials, Polymer 40 (1999) 1775–1779, doi:10.1016/S0032-3861(98)00402-9.
[161] P. Zhao, B. Xu, Y. Zhang, B. Li, H. Chen, Study on the twisted and coiled polymer actuator with strain self-sensing ability, ACS Appl. Mater. Interfaces 12 (2020) 15716–15725, doi:10.1021/acsami.0c01179.

[162] H. Yin, J. Zhou, J. Li, V.S. Joseph, Fabrication and properties of composite artificial muscles based on nylon and a shape memory alloy, J. Mater. Eng. Perform. 27 (2018) 3581–3589, doi:10.1007/s11665-018-3434-3.
[163] H. Yin, L. Tian, G. Yang, Design of fibre array muscle for soft finger with variable stiffness based on nylon and shape memory alloy, Adv. Robot. 34 (2020) 599–609, doi:10.1080/01691864.2020.1738272.
[164] L. Huang, X. Xie, H. Huang, J. Zhu, J. Yu, Y. Wang, Z. Hu, Electrospun polyamide-6 nanofiber for hierarchically structured and multi-responsive actuator, Sensors Actuators A Phys 302 (2020) 111793, doi:10.1016/j.sna.2019.111793.
[165] L. Saharan, Y. Tadesse, Robotic hand with locking mechanism using TCP muscles for applications in prosthetic hand and humanoids, in: Bioinspiration, Biomimetics, and Bioreplication 2016, 9797, 2016, p. 97970V, doi:10.1117/12.2219535.
[166] L. Wu, M. Jung de Andrade, R.S. Rome, C. Haines, M.D. Lima, R.H. Baughman, Y. Tadesse, Nylon-muscle-actuated robotic finger, in: Active and Passive Smart Structures and Integrated Systems 2015, 9431, 2015, p. 94310I, doi:10.1117/12.2084902.
[167] L. Saharan, L. Wu, Y. Tadesse, Modeling and simulation of robotic finger powered by nylon artificial muscles, J. Mech. Robot. 12 (2020), doi:10.1115/1.4044740.
[168] S. Kianzad, M. Pandit, J.D. Lewis, A.R. Berlingeri, K.J. Haebler, J.D.W. Madden, Variable stiffness structure using nylon actuators arranged in a pennate muscle configuration, in: Electroactive Polymer Actuators and Devices (EAPAD) 2015, 9430, 2015, p. 94301Z, doi:10.1117/12.2086799.
[169] V. Giovinco, P. Kotak, V. Cichella, C. Maletta, C. Lamuta, Dynamic model for the tensile actuation of thermally and electro-thermally actuated twisted and coiled artificial muscles (TCAMs), Smart Mater. Struct. 29 (2020) 025004, doi:10.1088/1361-665X/ab5e38.
[170] W. Owens, T.E. Bertorini, H.J. Holt, M. Shadle, A woman with limb swelling and pain, Neuromuscul. Case Stud. (2008) 581–583, doi:10.1016/B978-0-7506-7332-7.50103-3.
[171] K. Sears, C. Skourtis, K. Atkinson, N. Finn, W. Humphries, Focused ion beam milling of carbon nanotube yarns to study the relationship between structure and strength, Carbon N. Y. 48 (2010) 4450–4456, doi:10.1016/j.carbon.2010.08.004.
[172] R. Carloni, V.I. Lapp, A. Cremonese, J. Belcari, A. Zucchelli, A variable stiffness joint with electrospun P(VDF-TrFE-CTFE) variable stiffness springs, IEEE Robotics and Automation Letters 3 (2018) 973–978, doi:10.1109/LRA.2018.2793348.
[173] C. Gotti, A. Sensini, G. Fornaia, C. Gualandi, A. Zucchelli, M.L. Focarete, Biomimetic hierarchically arranged nanofibrous structures resembling the architecture and the passive mechanical properties of skeletal muscles: a step forward toward artificial muscle, Front Bioeng Biotech 8 (2020) 767, doi:10.3389/fbioe.2020.00767.